arXiv:2512.17312v2 [cs.CV] 1 Apr 2026

CodeDance: A Dynamic Tool-integrated MLLM for Executable Visual Reasoning

Qi Song[1,4*] Honglin Li[2,4*] Yingchen Yu[3] Haoyi Zhou[1] Lin Yang[2]
Song Bai[3] Qi She[4] Zilong Huang[3†] Yunqing Zhao[3†]
[1]Beihang University [2]Westlake University
[3]ByteDance Singapore [4]ByteDance China
zilong.huang2020@gmail.com yunqing.z.0817@gmail.com
CodeDance-VL.github.io

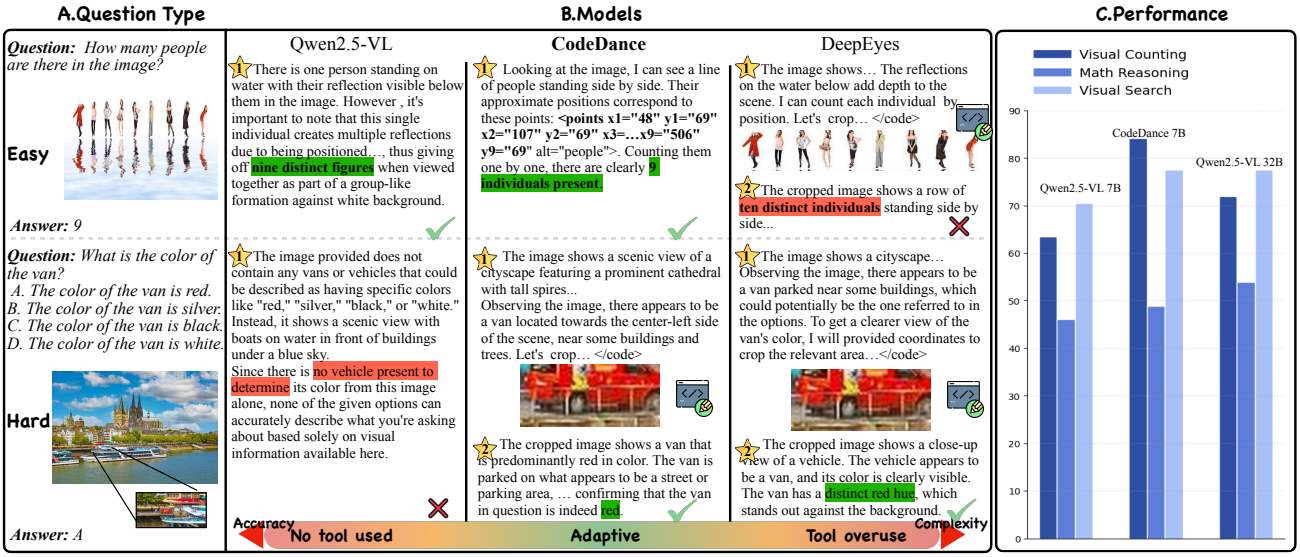


Figure 1. Motivation and effectiveness of dynamic tool invocation in CodeDance. **Left:** qualitative examples show that both tool underuse (unable to invoke tools on challenging tasks) and tool overuse (redundant calls on easy tasks) lead to hallucinated reasoning, incorrect answers, and unnecessary complexity (more reasoning turns and longer rollout time), whereas CodeDance dynamically invokes tools according to task difficulty to obtain correct solutions. **Right:** quantitative results show CodeDance-7B consistently surpasses all Qwen2.5-VL 7B baselines and exceeds the 32B version on several tasks.

Abstract

*Recent releases such as o3 highlight human-like "thinking with images" reasoning that combines tool use with stepwise verification, yet most open-source approaches still rely on text-only chains, rigid visual schemas, or single-step pipelines, limiting flexibility, interpretability, and transferability on complex tasks. We introduce **CodeDance**, which explores executable code as a general solver for visual reasoning. Unlike fixed-schema calls (e.g., only predicting bounding-box coordinates), CodeDance defines, composes, and executes code to orchestrate multiple tools, compute intermediate results, and render visual artifacts (e.g., boxes, lines, plots) that support transparent, self-checkable reasoning. To guide this process, we introduce a reward for balanced and adaptive tool calling, which balances exploration with efficiency and mitigates tool overuse. Interestingly, beyond the expected capabilities taught by atomic supervision, we empirically observe novel emergent behaviors during RL training: CodeDance demonstrates novel tool invocations, unseen compositions, and cross-task transfer. These behaviors arise without task-specific fine-tuning, suggesting a general and scalable mechanism for executable visual reasoning. Extensive experiments across reasoning benchmarks (e.g., visual search, math, chart QA) show that CodeDance not only consistently outperforms schema-driven and text-only baselines, but also surpasses closed models such as GPT-4o and larger open-source models.*

*Equal contribution. †Corresponding authors.

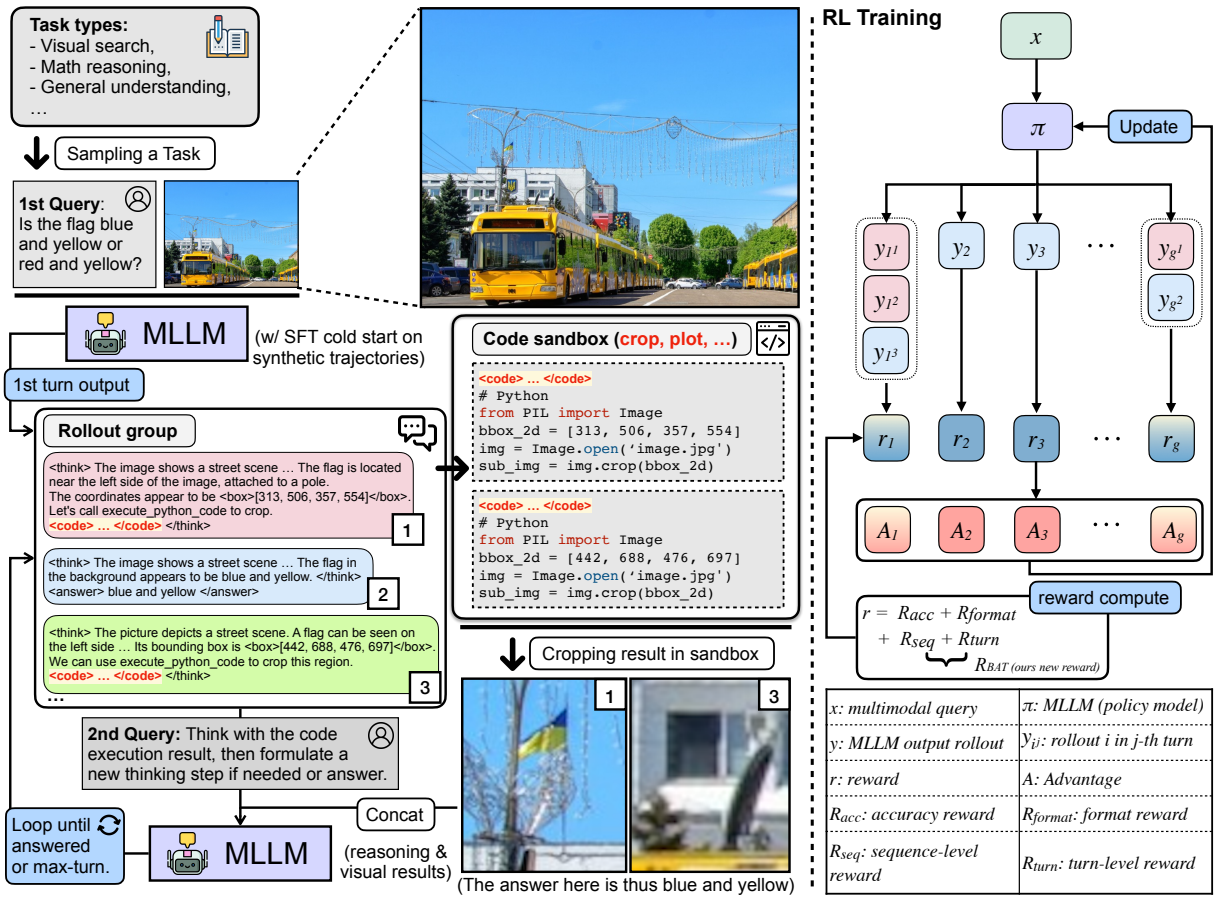


Figure 2. **Overview of our framework** that enables executable visual reasoning and invokes tool integration adaptively.

1. Introduction

Multimodal Large Language Models (MLLMs) have made rapid progress, showing strong capabilities in both visual perception and reasoning. By leveraging the language-centric chain-of-thought (CoT) mechanism [3, 40], models can decompose complex problems into intermediate steps, thereby improving performance on challenging tasks. However, when extended to visual tasks, traditional CoT relies on static context, preventing models from dynamically interacting with visual inputs or incorporating new observations during intermediate reasoning [6, 58], creating an information bottleneck that hinders multi-round focusing and validation. To address this, the o3 system [23] integrates the ability to actively seek new information through multiple tool invocations, supporting iterative reasoning over visual inputs and demonstrating strong perception and analysis.

Research gaps. While recent models have made notable progress, fundamental gaps remain unresolved. (1) Current approaches largely extend CoT into multimodal reasoning via text-only templates, failing to incorporate new observations, refine intermediate steps, or validate its reasoning against visual evidence [10, 14]. (2) In addition, o3 remains a proprietary black-box system: its internal mechanisms are inaccessible, its reasoning process is less transparent, and its outputs cannot be systematically studied or reproduced. (3) Most open-source systems incorporating visual reasoning remain restricted to predefined visual workflows, or rigid and schema-based pipelines (e.g., predicting bounding box coordinates for cropping operations), which are inherently inflexible and task-specific, limiting transfer to new tools and tasks [32, 33, 53, 57]. (4) Existing methods [55, 57] do not consider when a model should invoke tools, leading to tool underuse or overuse, as shown in Figure 1.

Consequently, the field still lacks an open and verifiable medium that is general across tools and tasks for multimodal reasoning, allowing MLLMs to dynamically compose tools, produce intermediate artifacts, and self-check their outputs in a transparent and reproducible manner. Addressing this gap is crucial for achieving task-adaptive, explainable, and transferable reasoning across complex real-world tasks.

In this work, we introduce **CodeDance**, a multimodal reasoning framework that leverages executable code as a unified medium for visual reasoning. Unlike prior schema-

Table 1. Experiment results on benchmarks including Counting, Visual Search, and General datasets. † denotes reproduced results.

Model	Visual Counting		Visual Search			General	
	CountBench	PixmoCount	V* Bench	HR-Bench 4K	HR-Bench 8K	ChartQA	CharXiv
Closed-Source MLLMs							
GPT-4o	87.9	-	67.5	65.0	59.6	86.7	47.1
Open-Source MLLMs							
Llava-OneVision-7B	82.3	54.4	72.7	68.5	60.0	80.4	27.1
Llava-OneVision-72B	-	60.7	73.8	66.3	60.9	83.7	-
InternVL2.5-8B	55.9	-	73.7	72.0	65.5	82.8	37.2
InternVL3-8B	80.3	-	70.2	70.5	70.0	86.1	38.3
InternVL3-78B	-	-	76.4	75.5	67.3	89.7	46.0
Qwen2.5-VL-72B	93.6	62.3	84.8	79.4	76.3	89.5	49.7
Qwen2.5-VL-32B	87.8	56.0	85.9	74.8	71.6	-	47.6
Qwen2.5-VL-7B	76.5	50.4	76.4	69.0	66.0	86.3	42.1
Tool-Integrated Open-Source MLLM							
Pixel Reasoner-7B	-	-	84.3	72.9	66.9	-	-
Deepeyes-7B†	80.4	57.2	90.4	74.8	71.9	78.2	-
Thyme-VL-7B	84.8†	-	82.2	77.0	72.0	86.1	44.2†
CodeDance-7B	91.2	77.1	84.8	75.2	72.3	87.5	44.1
Δ *vs. Qwen2.5-VL-7B*	**↑19.2%**	**↑53.0%**	**↑11.0%**	**↑9.0%**	**↑9.5%**	**↑1.4%**	**↑4.7%**

based pipelines with fixed operation templates, code enables the model to define, compose, and execute diverse visual–symbolic operations, producing both intermediate artifacts (e.g., cropped regions, plots, annotations) and final answers within a unified, verifiable reasoning process. To equip the model with fundamental skills, we curate a high-quality trajectory dataset and use supervised fine-tuning (SFT) to teach atomic capabilities such as counting, spatial grounding, and image annotation, enabling an iterative exploration-reflection reasoning process. Building on this foundation, we employ reinforcement learning (RL) to further enhance tool-based reasoning. A central challenge we identify is a *trade-off between exploration and selectivity*: naïve policies often overuse tools, incurring unnecessary steps, or underuse them, failing to leverage visual interactions when needed. To address this, we design a difficulty-adaptive tool-reward mechanism that adjusts incentives based on task complexity, encouraging longer operation chains for hard problems while discouraging unnecessary calls for simple ones. This aligns learning with the structure of multimodal tasks, resulting in more adaptive and transparent reasoning. Together, these components enable CodeDance to advance beyond rigid schema-based methods and offer an open, generalizable medium for executable visual reasoning.

Empirical observation of emergent behaviors. Although trained only on atomic operations, the framework exhibits behaviors beyond direct supervision during RL, including composing operations (e.g., localization followed by counting) and generating new procedural code for visual analysis. These behaviors arise from the base model's pretrained knowledge and are driven by adaptive rewards rather than explicit instruction, highlighting the scalability of dynamic invocation for more flexible and general reasoning.

Our contributions are summarized as follows: **(1)** We introduce CodeDance, a multimodal agent that can "think with images" by planning and composing visual–symbolic operations through executable code as a unified medium. To this end, we curate a 34K high-quality SFT dataset covering diverse atomic code capabilities (e.g., cropping, drawing, point plotting), and additionally design a difficulty-adaptive reward mechanism for RL, enabling multi-turn reasoning and balanced tool use. **(2)** We evaluate CodeDance on more than 10 multimodal benchmarks, spanning both general perception and complex reasoning (e.g., visual search, math reasoning). Across multiple benchmarks, it outperforms advanced closed models (e.g., GPT-4o) and larger open-source baselines (e.g., Qwen2.5-VL-32B), demonstrating strong perception and reasoning capabilities, and broad generalizability. **(3)** Despite being trained only on atomic operations, CodeDance empirically exhibits emergent behaviors during RL training, including spontaneous novel tool routines, unseen operation compositions, and cross-task transfer to novel tasks. These promising observations highlight the scalability and generality of our framework, and we empirically verify them in ablation studies.

2. Related Works

Multimodal reasoning and tool invocation. Building upon text-based chain-of-thought (CoT) reasoning [40, 47], researchers have extended intermediate reasoning steps to multimodal settings [48, 57] including counting [52], localization [42], charts [17], and visual math [5]. To enhance reasoning capabilities, recent works integrate external tools through reasoning-and-acting frameworks [45, 47], learned API usage [26], and multimodal agents that orchestrate OCR, detection, and editors [29, 41]. ViperGPT [34] compiles queries into executable programs. Recent models like OpenAI's o3 [23] integrate comprehensive tool capabilities directly into reasoning chains, trained via RL on large-scale CoT data. Other approaches include RL-based tool invocation [32, 57] and SFT-based methods [38]. However, challenges remain such as ad-hoc operations, sparse supervision, limited task coverage and lack of comprehensive evaluation. We diverge from prior work by pursuing code as a general medium to execute multimodal reasoning across diverse atomic abilities.

Adaptive thinking capability of MLLMs. Recent work on adaptive reasoning in LLMs explores how models can dynamically decide when and how much to think [50] instead of relying on fixed chain-of-thought steps. Approaches such as adaptive thinking [35, 43], concise reasoning [31], and learn-to-switch frameworks [54] show that LLMs can selectively perform deeper reasoning only when necessary, improving efficiency while preserving accuracy. Meanwhile, MLLMs can extend this: recent fast–slow vision-language reasoning demonstrates that models can also adjust reasoning depth based on visual–textual difficulty [44]. However, these methods focus mainly on adjusting internal reasoning depth rather than deciding when visual operations or tools should be invoked. This limitation motivates the investigation of adaptive tool calling for multimodal reasoning, where MLLMs must think with visual inputs effectively.

3. Methodology

3.1. Overview

Think-execute-feedback as reasoning unit. An overview of our framework is shown in Figure 2. Given a multimodal user query (including a text prompt and an image), the policy model (an MLLM) produces rollouts interleaving natural-language reasoning with executable code (e.g., cropping, plotting). Code is executed in a separate sandbox, and the resulting visual evidence (e.g., a cropped region) is concatenated with text to refine reasoning in the next turn or yield the final answer (e.g., "blue and yellow" in Figure 2).

We define a *think–execute–feedback* cycle as the minimal reasoning unit under a policy model π, where each turn comprises (i) the current query and reasoning trace, (ii) a candidate action, and (iii) the resulting observation after code execution. Formally, a trajectory is:

$$\tau = \big((s_{t_1}, a_{t_1}, s'_{t_1}), \ldots, (s_{t_{M-1}}, a_{t_{M-1}}, s'_{t_{M-1}}), (s_{t_M}, a_{\text{ans}})\big),$$

where t is the time step. $s_t = (x, o_t, \epsilon_t)$ contains the original query x, the accumulated reasoning trace o_t, and interpreter feedback ϵ_t. Actions a_t are drawn from a space including tool calls (code snippets) and a terminal answer; executing code yields an observation and updates the state to s'_t. By iterating $a_t \sim \pi(\cdot \mid s_t)$ until a final answer is produced or a maximum turn budget M is reached, each turn becomes an executable and verifiable reasoning unit. Building on this formulation, Section 3.2 details the curation of a high-quality trajectory dataset encompassing diverse atomic abilities. This dataset provides the foundation for initializing the policy model through SFT, before advancing to RL.

Table 2. Comprehensive results across math reasoning benchmarks. † denotes results from their official papers.

Model	Math-Benchmark			
	MathVision	MathVista	MathVerse	WeMath
Larger MLLMs without Reasoning				
GPT-4o	36.5	63.4	35.3	44.2
Qwen2.5-VL-72B	38.1	74.8	57.6	-
Open-source Reasoning MLLMs				
R1-Onevision-7B †	29.9	64.1	40.0	-
R1-VL-7B†	24.7	63.5	40.0	-
Open-source General MLLMs				
InternVL2.5-8B	22.0	64.4	39.5	23.9
Llava-OV-7B	18.4	63.2	26.2	17.3
Qwen2.5-VL-7B	25.0	68.1	45.1	35.4
DeepEyes-7B	26.6	70.1	47.3	38.9
CodeDance-7B (Ours)	29.6	70.3	46.8	39.6

Policy optimization via verifiable evidence. In the RL stage, we require a policy optimization method that can compare multiple rollouts and update the model accordingly. In our case, Group Relative Policy Optimization (GRPO) [28] provides a natural baseline, as it directly normalizes rewards across sampled trajectories without relying on a separate value network. However, standard GRPO assigns a uniform advantage to all tokens within a trajectory, which limits its effectiveness for multi-turn tool reasoning requiring intermediate correction. To address this, we extend the reward design with sequence-level and turn-level components. In particular, each rollout is evaluated with a composite reward r that integrates outcome and tool-related signals (also see Figure 2, right side):

$$r(\tau) = R_{\text{acc}}(\tau) + R_{\text{format}}(\tau) + R_{\text{BAT}}(\tau),$$

where R_{acc} denotes final-answer correctness and R_{format} enforces format compliance, respectively. In our design, we introduce a two-level reward R_{BAT} (**Reward for Balanced Adaptive Tool Calling**) that advocates adaptive tool calling based on the task difficulty. In particular, it decomposes

into a sequence-level R_{seq} and a turn-level R_{turn}, balancing task difficulty with step-wise tool calling correctness. Subsequently, the advantage A is written as:

$$A(\tau) = A_{\text{seq}}\big(R_{\text{acc}}, R_{\text{format}}, R_{\text{seq}}\big) + A_{\text{turn}}\big(R_{\text{turn}}\big).$$

Next, we show that this formulation combines global, step-level trajectory outcomes with local, turn-level execution feedback, producing more adaptive tool invocation.

Sequence-level adaptive reward for code-invocation. Simply rewarding every successful tool call can lead to degenerate behaviors such as tool spamming or reward hacking on trivial problems (see Appendix Figure 12), which may hinder the reasoning performance (ablation studies in Table 3). To address this, we design an adaptive reward that conditions tool incentives on the group-level accuracy μ_{acc}: when most rollouts already solve the task correctly (indicating that the problem is relatively easy or solvable without additional tool assistance), further invocations are discouraged. In contrast, low μ_{acc} encourages additional exploration. Formally, the sequence-level reward is as follows:

$$\begin{aligned} R_{\text{seq}} &= \Big(0.5 + 0.5 \cdot \mathbb{I}_{R_{\text{acc}}(\tau)>0}\Big) \cdot d \cdot \frac{N_{\text{succ}}(\tau)}{N_{\text{total}}(\tau)}, \\ d &= \sigma\big(\gamma(0.5 - \mu_{\text{acc}})\big) - \delta, \sigma(z) = \frac{1}{1+e^{-z}}, \end{aligned} \tag{1}$$

where $N_{\text{succ}}(\tau)$ and $N_{\text{total}}(\tau)$ denote the numbers of successful and total tool calls in trajectory τ, and d is a group-accuracy–dependent scaling factor that suppresses rewards for unnecessary tool calls on easy queries (high μ_{acc}) and amplifies rewards for tool-assisted solutions on hard queries (low μ_{acc}), thereby enabling adaptive tool invocation. Here, γ and δ are hyper-parameters controlling the strength: higher μ_{acc} reduces d (discouraging redundant calls), while lower μ_{acc} increases d (promoting exploration). We set $\gamma = 4$ and $\delta = 0.2$ in our main experiments. See our Appendix 8.2 for discussion of these hyper-parameters.

Turn-level execution reward. To penalize failed executions and provide dense correction signals, we introduce a turn-level reward. For each turn m, an immediate penalty $r_{\text{turn},m} = -0.5$ is assigned if the code execution fails, and 0 otherwise. To capture long-term effects, we recursively redefine $r_{\text{turn},m}$ as the accumulated discounted return:

$$R^m_{\text{turn}} = r^m_{\text{turn}} + \beta \cdot R^{m+1}_{\text{turn}}, \quad A^m_{\text{turn}} = \frac{R^m_{\text{turn}} - \mu_{\text{batch}}}{\sigma_{\text{batch}}}. \tag{2}$$

Here, R^m_{turn} denotes the discounted cumulative turn-level return, β is a discount factor, and $\mu_{\text{batch}}, \sigma_{\text{batch}}$ denote the batch-wise mean and standard deviation of R_{turn}, respectively. This turn-level reward discourages credit assignment to incorrect intermediate reasoning steps, even when the final answer is correct, and it helps mitigate entropy collapse during training (Figure 5). The final advantage is obtained by combining the resulting A_{turn} with the sequence-level advantage A_{seq} (from outcome-level rewards, see Appendix).

Together, the group-adaptive R_{seq} evaluates the quality of an *entire* trajectory, while R_{turn} assesses the correctness of *individual* tool calls. This complementary design, which we term $R_{\text{BAT}} = R_{\text{seq}} + R_{\text{turn}}$, mitigates reward hacking, balances efficiency with necessary exploration, and yields more robust multimodal reasoning policies. We discuss more design choices and results in Figure 5.

3.2. Data Engineering

In our design, the lack of high-quality, multi-turn, multimodal reasoning datasets that advocate adaptive tool calling with interleaved code trajectories remains a major barrier for training. To address this, we construct a 34k dataset for cold start, featuring **(1)** the reasoning trajectories that include code execution results appended as **visual evidence** in training, and **(2) adaptive tool invocation** based on the level of questions. For easy questions, the model is encouraged to answer directly without any reasoning process. For hard questions, we enable code-based tool integration for executable reasoning. Practically, to mitigate the issue of tool spamming, we ensure that the pipeline follows a two-step design: **(i) weak-to-strong filtering**, where public resources (e.g., SA1B, GEOqa_plus, MMK12) are automatically filtered and stratified by difficulty using Qwen2.5-VL-7B; and **(ii) multi-turn atomic supervision**, where hard cases are decomposed into trajectories covering three categories: fundamental image transforms (crop, resize), mathematical computation (measurement, algebra, aggregation), and open-ended visual editing (drawing, annotation, etc.). Each trajectory is further verified by a stronger MLLM (e.g., Qwen2.5-VL-72B) to cross-validate the correctness. The query, code, and response are embedded as follows:

Multimodal CoT trajectories for cold-start

Query: <IMAGE> Is the flag blue and yellow or red and yellow?
Response: The image shows..., Let's call execute_python_code: \n <code>from PIL import Image \n img = Image.open('img.jpg')...</code>. Appending compiling results... \n <answer>blue and yellow</answer>
Example atomic abilities (<code></code>):

Cropping
```
from PIL import Image
img =
Image.open('img.jpg')
bbox_2d = [463, 168,
500, 217]
sub_img =
img.crop(bbox_2d)
x1,y1,x2,y2 = bbox_2d
bbox_w = x2 - x1
bbox_h = y2 - y1
```

Annotate
```
from PIL import Image,
ImageDraw
boxes = [[0, 0, 223, 223],
[244, 0, 467, 223], [473, 0, 644,
223] ...]
img =Image.open(.)
draw =
ImageDraw.Draw(.)
for(x1,y1,x2,y2)in
boxes:draw.rectangle((
```

Pointing
```
import cv2
points=[[462, 184]]
img = cv2.imread(img)
radius = 6
cv2.circle(img, (x, y),
radius * 2, (255, 0,
0), -1)
cv2.putText(img,
str(idx+1), (x + radius
+ 3, ...)
```

These trajectories provide verifiable supervision of the atomic skills used for SFT as cold-start. In Appendix 7.1,

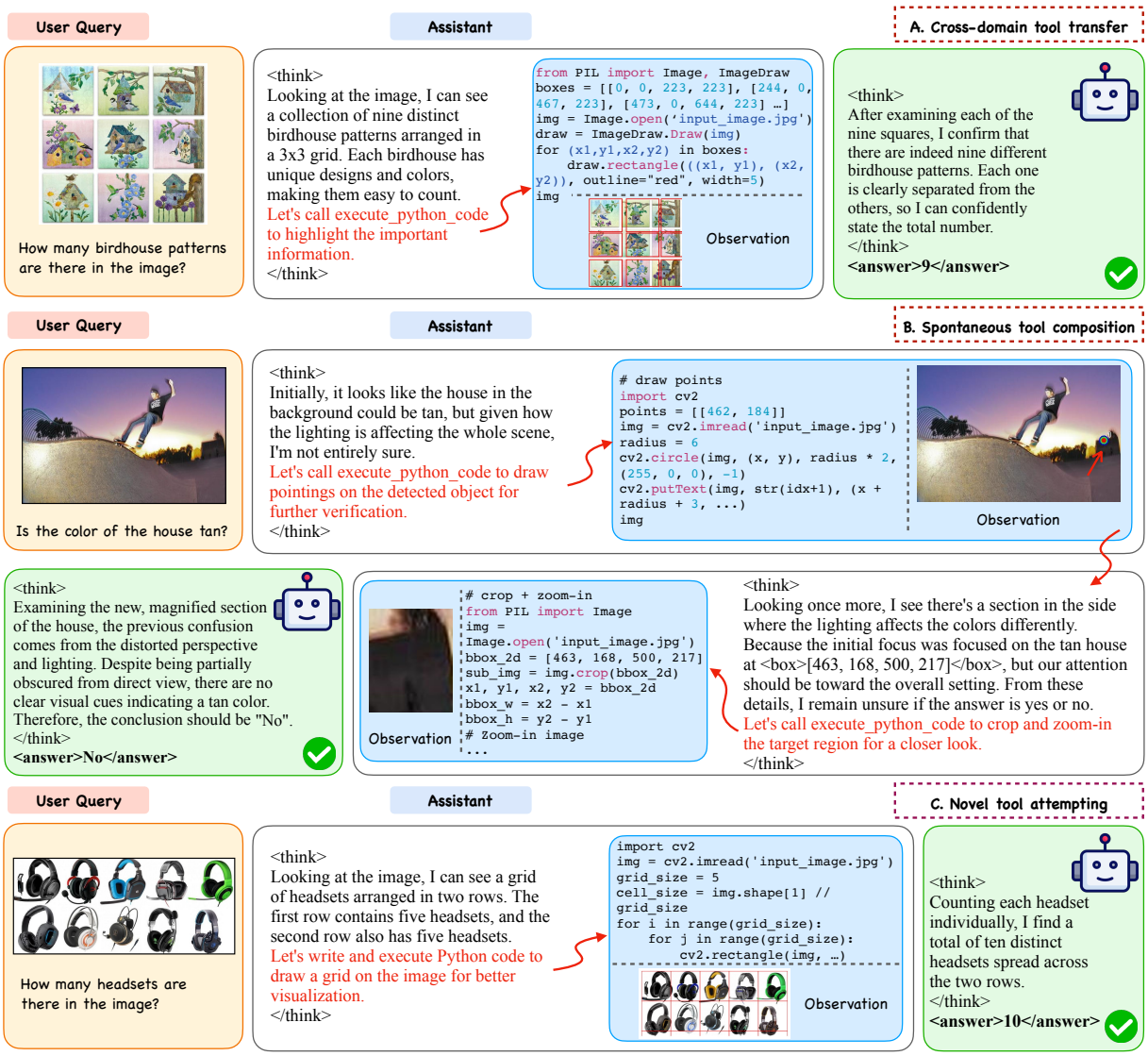


Figure 3. **Intriguing reasoning trajectories emerge during RL.** These behaviors are absent from the SFT data and arise from pretrained knowledge further shaped by RL, reflecting our design of adaptive tool invocation. These emergent patterns motivate our scaling study in Figure 4, where we further examine whether these capabilities strengthen with larger data, longer training, and bigger models.

we provide the comprehensive recipe on trajectory synthesis, filtering and code integration for SFT data, with additional examples for RL training.

4. Experiments

Implementation Details. Our method is designed to be seamlessly integrated into popular MLLM architectures. In our experiments, we mainly build on Qwen2.5-VL-7B [1] as the base model, and compare against both open-source reasoning MLLMs (e.g., DeepEyes [57]) and advanced closed models (e.g., GPT-4o) across four benchmark categories: math reasoning (MathVista [18], MathVision [36], MathVerse [51], WeMath [25], general reasoning (ChartQA [19]), counting (PixmoCount [8], CountBench [24]), and visual search (V* Bench [42], HRBench [37]). For training, we adopt SWIFT [56] for SFT and VeRL [30] for RL. We empirically set $\gamma = 4$, $\delta = 0.2$, and $\beta = 0.2$. To ensure a fair comparison, we adopt VLMEvalKit [9] as the evaluation framework. The max-turn set to 10 for evaluation and 6 for training.

4.1. Visual Reasoning Tasks

As shown in Table 1, CodeDance attains strong results across diverse visual reasoning benchmarks, including counting, visual search, and chart understanding. Notably, it achieves state-of-the-art performance on Counting and ChartQA, outperforming the baseline by a large margin and surpassing even larger models. These improvements

Table 3. Ablation study on reward design. We report accuracy, average turns, and execution success rate on different reasoning benchmarks.

Components	CountBench Acc. / Turns	Pixmo Acc. / Turns	V* Bench Acc. / Turns	HR 4K Acc. / Turns	HR 8K Acc. / Turns	MVsion Acc. / Turns	MVerse Acc. / Turns	Avg. Acc. / Turns	Succ.
SFT Cold-Start (w/o RL)	85.3 1.27	66.9 1.39	82.7 2.01	72.1 1.17	67.1 1.09	23.0 2.84	41.4 2.19	62.6 1.71	0.96
RL with R_{acc}+R_{format}	89.0 1.22	72.9 1.54	84.8 1.00	74.5 1.03	71.1 1.04	28.6 1.97	46.5 2.17	66.8 1.42	0.97
+R_{DeepEyes} [57]	83.1 2.35	70.6 2.25	**86.4** 2.01	**75.8** 2.07	70.3 2.12	26.6 2.65	46.3 2.37	65.6 2.26	0.97
+R_{BAT}-w/o Turn-level Reward	87.4 1.01	**78.8** 1.00	**86.4** 1.12	75.1 1.07	70.1 1.08	28.6 1.97	46.3 2.41	67.5 **1.38**	0.91
+R_{BAT} (CodeDance)	**91.2** 1.00	77.1 1.00	84.8 1.00	75.2 1.06	**72.3** 1.06	**29.6** 2.19	**46.8** 2.35	**68.1** **1.38**	**0.99**

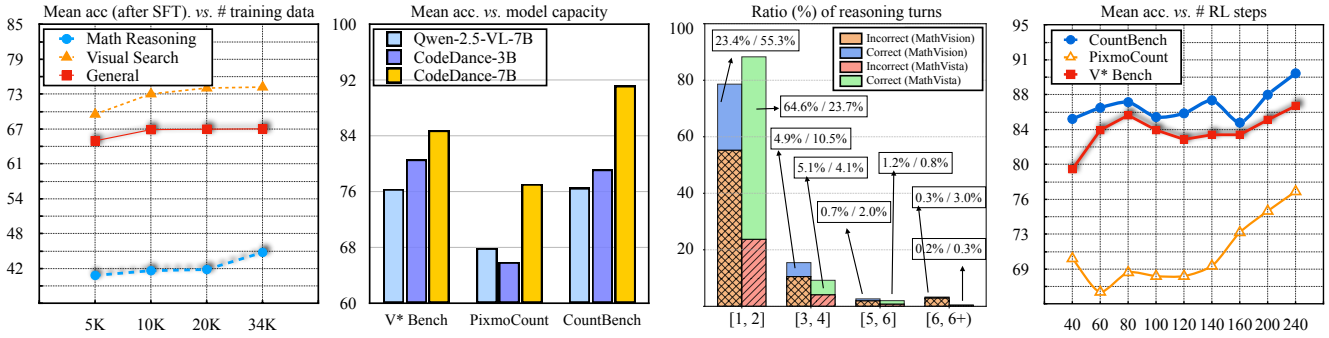


Figure 4. Scaling up compute budget on four dimensions: dataset size for SFT, model capacity, max-turns during inference and RL steps.

highlight the advantage of executable code as a reasoning medium: by delegating fine-grained visual analysis to code-based tools, it extends beyond the raw perceptual capacity of the base model, yielding gains that cannot be achieved through scaling alone, particularly on perception-heavy tasks.

4.2. Math Reasoning Tasks

In mathematical reasoning, CodeDance shows consistent gains over open-source baselines (see Table 2). For instance, it improves accuracy on MathVision from 25.0 to 29.6 (+18.4%) and on WeMath from 35.4 to 39.6 (+11.9%), while maintaining competitive results on other benchmarks. These tasks require precise symbolic manipulation and stepwise calculations, which are naturally supported by executable code. By externalizing intermediate steps into verifiable scripts, CodeDance demonstrate strong accuracy and reliability than relying solely on internal approximation.

4.3. Key Findings: Emergent Behaviors during RL

Throughout the RL process, we observe novel and surprising empirical findings (shown in Figure 3) that go beyond the atomic supervision provided during SFT. These findings point toward the scalability of code as a general reasoning medium, and we empirically study the potential in Figure 4.

Cross-domain tool transfer. We observe an emergent generalization ability in our CodeDance, where visual operations defined for a specific task can be repurposed in other contexts. For example, the bounding-box operation was initially designed to highlight particular results within chart tasks in our SFT data. However, the model demonstrates the ability to adapt this operation for counting tasks during RL training: e.g. In Figure 3A, the MLLM assistant first localizes all candidate objects by drawing bounding boxes, then validates the correctness of each localization, and subsequently derives the final count. Additional tool transfer trajectories can be found in Figure 14. Such behavior indicates that task-specific visual operations are not rigidly bound to their original purpose, but can be flexibly generalized to support broader multimodal reasoning scenarios. This suggests that visual operations such as bounding boxes can function as general *reasoning primitives*, serving as transferable building blocks across heterogeneous tasks.

Novel tool composition of learnt capabilities. Although during SFT data curation and collection, each task was restricted to a single predefined tool or coding operation, we observe that after post-training the model develops the ability to compose multiple atomic operations to address more complex tasks beyond the training coverage: In Figure 3B, to validate the color of the house, the MLLM assistant first applies a pointing operation to check the house position correctness, then use crop with zoom-in to focus on fine-grained details. Similarly, we show example in Appendix Figure 15 that the bounding-box drawing and crops

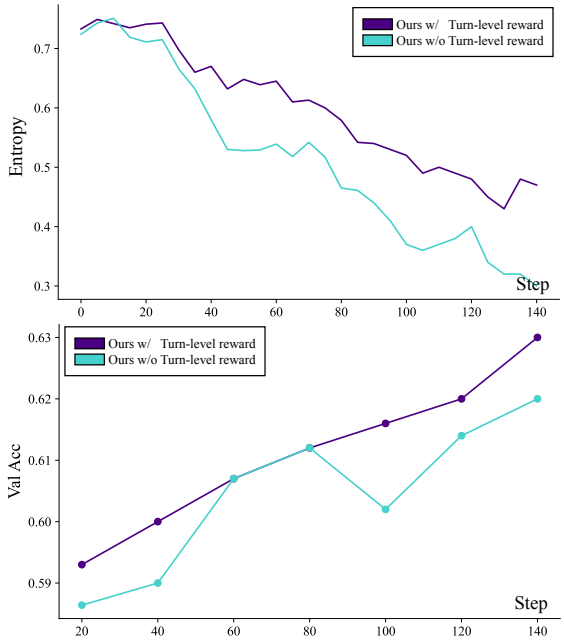


Figure 5. Entropy and validation accuracy of model's generation.

are combined to focus and solve the chart reasoning task. These observations highlight the emergence of novel tool compositions, where elementary visual operations are flexibly combined to form higher-level reasoning strategies.

Incentivizing emergence of novel unseen capabilities. Interestingly, we also find that the model exhibits a certain potential to generate tool codes not explicitly defined in the SFT data. These codes appear to be drawn from the model's pretraining knowledge and are occasionally activated during the post-training stage. For example, when asked to count the number of headsets in an image (Figure 3C), the MLLM does not directly respond with a number, but instead attempts to write Python code with OpenCV functions (e.g., using `cv2.rectangle` to overlay a grid for better visualization). This observation suggests that, beyond reproducing SFT-defined behaviors, the model attempts to reuse and adapt pretrained capabilities (e.g. complex OpenCV operations) to support reasoning tasks, indicating a certain potential for more flexible tool usage.

4.4. Ablation Studies

Validation of reward design. We compare three reward designs for guiding tool usage (Table 3): (i) GRPO-reward (*Outcome-level reward*) focuses only on final-answer correctness. While it shortens interaction turns, it discourages tool usage and underperforms on complex tasks. (ii) *DeepEyes reward* grants positive signals for every successful tool execution upon accurate answer. Although this encourages exploration, it also leads to tool overuse on trivial problems, increasing turns without consistent accuracy gains. A qualitative example is provided in Appendix Figure 12. (iii) *Our reward* R_{BAT} for adaptive tool-call balances the two extremes by penalizing redundant calls and rewarding selective, high-impact interactions. As Table 3, outcome-level GRPO under-utilizes tools, and the *DeepEyes reward* inflates turns without reliable accuracy improvement. Furthermore, removing the turn-level reward severely degrades the execution success rate. Overall, the full R_{BAT} achieves the best overall accuracy while avoiding unnecessary tool use, consistently surpassing both baselines.

Validation on scaling up the compute budget. Motivated by the emergent behaviors observed in Figure 3, we further examine whether CodeDance continues to benefit from scaling along four axes, as summarized in Figure 4. **(i) Training dataset size** for SFT, including Math Reasoning (MathVision, MathVerse, MathVista), Visual Search (V*, HR 4K, HR 8K), and General (ChartQA, MMVet, MMStar). We consistently observe that enlarging the SFT dataset from 5K to 34K yields steady accuracy gains, showing that both tool selection and symbolic planning benefit from broader coverage. **(ii) Increasing model capacity** from 3B to 7B substantially boosts reasoning benchmarks such as counting and search, where CodeDance-3B even outperforms a stronger 7B model. **(iii) Extending RL training** up to 240 steps further improves accuracy without overfitting, supported by our reward design R_{BAT}. **(iv) Increase the inference turn budget**. Although we set a maximum of 6 turns of the RL training, we observe that allowing more turns at inference (10) continues to improve reasoning performance. In experiments, the model achieves additional gains even beyond 6 turns (0.3%), suggesting that the learned policy can generalize to longer reasoning horizons.

Empirical study on inference entropy and accuracy. In Figure 5, we evaluate the impact of incorporating turn-level reward (R_{turn}) on training dynamics and generalization. We study the impact of turn-level reward in R_{BAT} on several benchmarks, mainly including visual search (V^* Bench), math reasoning (MathVista, MathVerse, MathVision), and counting benchmarks (PixmoCount and CountBench). (a) *Entropy:* Without R_{turn}, policy entropy collapses quickly because flawed intermediate steps may still lead to correct final answers, reinforcing shortcuts and limiting exploration [49]. With R_{turn}, intermediate penalties delay collapse, sustaining exploration. (b) *Validation Accuracy:* The additional corrective signals prevent premature convergence and translate into consistently higher accuracy, showing that local feedback improves global generalization.

5. Discussion

We present CodeDance, a task-aware, difficulty-adaptive MLLM that uses executable code for tool-integrated visual reasoning. By allowing models to define and execute code, CodeDance enables flexible reasoning with interpretable intermediate evidence, while promoting adaptive tool calls and discouraging tool spamming. During RL, CodeDance

exhibits emergent behaviors beyond supervised skills, including novel tool routines, compositional strategies, and cross-domain transfer. We further verify its scalability, observing clear and consistent gains with increased compute budget. Even at the 7B scale, CodeDance achieves competitive performance across diverse benchmarks, highlighting code-based, difficulty-adaptive reasoning as a scalable and transferable paradigm for multimodal and agentic AI.

Acknowledgements

This work was supported by the grants from the Natural Science Foundation of China (62202029), and Young Elite Scientists Sponsorship Program by CAST (No. 2023QNRC001).

Appendix

This appendix serves to enhance the reproducibility and transparency of our work by supplementing the main paper with critical technical details and experimental analyses. We provide additional implementation details (e.g., pipeline and examples of the trajectory construction, training setups, and hyperparameters), further descriptions and comparisons of our curated datasets and prompt templates, additional qualitative and quantitative results on various benchmarks, and extended discussions on design choices, broader impacts, limitations and future works.

Contents

1. Introduction **2**

2. Related Works **4**

3. Methodology **4**
3.1. Overview 4
3.2. Data Engineering 5

4. Experiments **6**
4.1. Visual Reasoning Tasks 6
4.2. Math Reasoning Tasks 7
4.3. Key Findings: Emergent Behaviors during RL 7
4.4. Ablation Studies 8

5. Discussion **8**

6. Additional implementation details **9**
6.1. Hyperparameters in training and inference . . 9
6.2. Implementation of Code sandbox 9
6.3. Implementation of standard GRPO 10

7. Data engineering **10**
7.1. Dataset curation 10
7.2. Prompt templates 11

8. Additional empirical studies **12**
8.1. Visualization of sequence/turn-level rewards 12
8.2. Hyperparameters in our method 15
8.2.1 . Sensitivity of R_{BAT} Hyperparameters 15
8.2.2 . Effective range and bounds of $d(\mu_{\text{acc}})$ 15
8.2.3 . Hyperparameter over (γ, δ) 15
8.3. Analysis of Reasoning Depth 15

9. Additional qualitative results **16**
9.1. Failure cases observed in our experiments . . 17
9.2. Additional novel reasoning trajectories . . . 17

10Discussion **18**

11Broader impact **19**

12Limitations and future work **19**

6. Additional implementation details

6.1. Hyperparameters in training and inference

In Table 4, we present the additional hyperparameters used for training our model on the multimodal reasoning tasks. We primarily adhere to the same settings as Qwen2.5-VL [2], and these parameters are mostly applied across other tasks.

Table 4. Hyperparameters used in training/inference.

	Param. Name	Value / Type
SFT	Batch size	128
	Learning rate	5e-5
	Warmup ratio	0.05
RL	Numerical precision	BF16
	Global batch size	256
	Rollout	8
	Total epochs	1
	Time	∼2 Days
Inference & Eval	Deployment platform	vLLM [15]

6.2. Implementation of Code sandbox

To safely execute model-generated programs during training and evaluation, we run all Python code in an internal sandboxed environment. Each execution instance is assigned an isolated working directory and a dedicated namespace for variables, functions, and imports; for multimodal tasks, input images are stored in the corresponding temporary directory and are only visible within that instance. This design avoids interference across concurrent rollouts and confines state to a single trajectory.

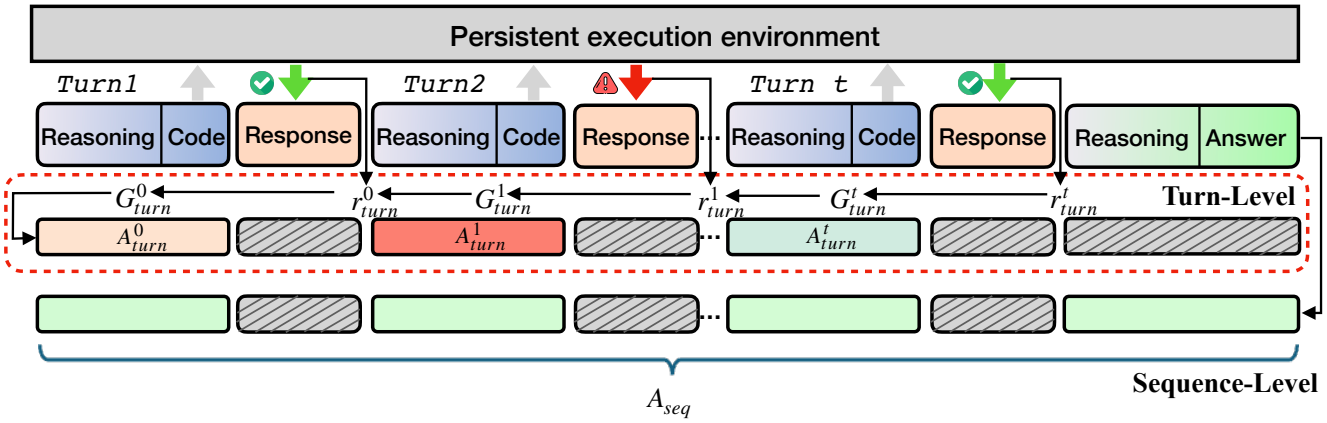


Figure 6. Interaction of our reward design R_{BAT} with the code sandbox (i.e., the execution environment).

Before running user code, the sandbox disables a small set of APIs that may compromise the stability (e.g., blocking user input, direct process termination), and treats each execution as an atomic transaction: if a run fails or is interrupted, partial updates are discarded and the logical state of the instance reverts to the last successful step. We further enforce a strict per-call wall-clock time limit (15s by default); when the limit is exceeded, the current execution is aborted and a timeout status is returned. Finally, the sandbox centralizes observability by capturing structured stdout/stderr logs and graphical outputs produced by common plotting libraries (e.g., `matplotlib`, `PIL`), which are then fed back to the model as textual and visual observations. An illustration of interaction with the code sandbox is shown in Figure 6.

6.3. Implementation of standard GRPO

Here, we reveal additional implementation details regarding the RL algorithm used in our work. Group Relative Policy Optimization (GRPO, Shao et al. [28]) has demonstrated strong effectiveness across diverse tasks, particularly in multi-turn tool call agents and "thinking with images" system [10, 11, 32, 57]. Unlike PPO [27], GRPO removes the need for a separate value network by directly computing advantages from the normalized rewards of G sampled solutions. Formally, let $\pi_{\theta_{\text{old}}}$ and π_θ denote the policy model (parameterized by θ) before and after the update, respectively, both defined over the action/token space at each position. For a question q sampled from a task dataset $\mathcal{Q}$, a group of G candidate solutions $\tau_i \sim \pi_{\theta_{\text{old}}}$ are rolled out and evaluated with a reward function $r(\cdot)$. Building on the clipped surrogate objective of PPO, we write the objective $\mathcal{J}$ in an empirical expectation form:

$$\mathcal{J}_{\text{GRPO}}(\theta) = \mathbb{E}_{q\sim\mathcal{Q},\,\{\tau_i\}_{i=1}^{G}\sim\pi_{\theta_{\text{old}}}(\cdot|q)}\left[\frac{1}{G}\sum_{i=1}^{G}\frac{1}{|\tau_i|}\right. \tag{3}$$
$$\left.\sum_{t=1}^{|\tau_i|}\min\Big(r_{i,t}A_i,\text{clip}(r_{i,t},1-\varepsilon,1+\varepsilon)A_i\Big)\right].$$

where $r_{i,t} = \frac{\pi_\theta(\tau_{i,t}|q,\tau_{i,<t})}{\pi_{\theta_{\text{old}}}(\tau_{i,t}|q,\tau_{i,<t})}$, $\varepsilon = 0.2$ by default, and clip$(\cdot)$ denotes the clipping operator for stability. We omit the KL penalty here for simplicity. The normalized within-group reward then defines the advantage A_i of solution τ_i:

$$A_i = \frac{r(\tau_i) - \text{mean}(\{r(\tau_j)\}_{j=1}^{G})}{\text{std}(\{r(\tau_j)\}_{j=1}^{G})}. \tag{4}$$

We mostly followed the original implementation of GRPO [28] to compute outcome-driven advantage A_{seq}.

7. Data engineering

7.1. Dataset curation

Here, we firstly discuss several related works on data synthesis for MLLM training to complete the related works. Then, we show details of our dataset curation pipeline.

Background: Synthetic reasoning data for MLLM post-training. High-performance MLLMs require substantial instruction-following training data with detailed reasoning trajectories. Recent approaches include converting existing datasets using fixed templates [7, 39] or distilling knowledge from strong teacher models [4, 38, 55], with a focus on developing specific capabilities such as visual-centric reasoning [16] and mathematical problem-solving assisted by visual cues [5, 12]. However, several limitations persist in existing approaches: (i) tool-grounded verification

mechanisms are often absent, and (ii) visual operations are typically limited to fixed schema such as cropping or zooming in [32, 57]. In contrast, we synthesize and curate training data with comprehensive reasoning trajectories and tool/code-assisted responses across a wide range of atomic visual operations, employing enhanced process supervision including multi-judge filtering and consistency validation. This leads to "thinking with images" reasoning capability [23] with competitive performance while requiring substantially less training data.

Synthesize high-quality cold-start trajectories for tool-integrated reasoning (TIR). An overview of the curation pipeline as a supplement of the main paper is shown in Figure 7 and a detailed example is in Figure 8. In addition, the dataset used for our trajectory synthesis is primarily composed of the following datasets:

- **Mathematical Reasoning**: MMK12 [22], Retool [10].
- **Table Data**: ChartQAPro [21], chartgemma [20].
- **Natural Images**: SA1B [13].
- **General Data**: Mulberry [46].

For the RL training, our data mainly comes from Deepeyes [57], SA1B [13] and PixmoCount train [8].

7.2. Prompt templates

Prompt templates used in SFT data synthesis. To ensure the reliability and consistency of synthesized data, we design a set of standardized prompt templates tailored for different stages of the vision-language data pipeline. These templates serve complementary purposes: **(i) In Table 5:** assessing the informativeness of candidate images to guarantee sufficient visual complexity for fine-grained reasoning; **(ii) In Table 6:** labeling and locating the objects that most match the question. **(iii) In Table 7:** validating the quality of automatically generated visual question–answer pairs; **(iv) In Table 8:** enforcing a structured step-by-step reasoning process with explicit final answers; and **(v) In Table 9:** enhancing reasoning accuracy by incorporating code interpreter support for precise numerical or logical calculations. Together, these prompt templates provide a comprehensive and systematic framework for controlling data quality during synthesis, thereby improving the robustness and utility of the resulting multimodal datasets.

Prompt templates used in RL training. We provide the RL training prompt template in **Table 10**. This template illustrates the input–output format and executable code constraints used during RL rollouts, offering additional transparency and reproducibility of our training setup.

Example SFT training data. To better illustrate the construction of SFT data, we provide representative examples of atomic operations. As shown in Figure 9, the top trajectory corresponds to a two-turn reasoning process, where the model iteratively performs cropping, observes intermediate results, and reflects on the correctness before locating the accurate price tag of a specific toothbrush. In contrast, the bottom trajectory demonstrates a single-turn process, in which the model directly identifies the phone number from a cropped sign. These cases exemplify how SFT data captures both multi-step and single-step reasoning, integrating tool invocation, visual observation, and answer generation.

Table 5. Prompt template for assessing image informativeness.

You are an expert vision-language analyst. **Task** 1. Observe the entire image. 2. Decide whether the picture meets **all Four conditions** below: A. Diversity – Contains $\geq$ 4 different object categories **or** $\geq$ 6 individual objects. B. Distinguishability – Includes at least one object that is mostly un-occluded, covers ¡ 30% of the image area, and is not repeated by many visually identical copies. C. Zoom-in Benefit – For that object (or another), some informative fine-grained detail (e.g., printed text, small logo, numerical value, subtle texture, or facial expression) would become noticeably clearer if the region were enlarged. In other words, a close-up view would materially help a downstream model answer a question about that object. D. Is it suitable to come up with some VQA questions that require fine-grained understanding? 3. If **all** A, B, C, D are satisfied, Please respond with "True" or "False".

Table 6. Prompt template for bbox generation.

Please detect the entire object that most matches the question in the image. **Question:** `{question}` If the target is part of an object, you need to give the bbox of the entire object. For each object, return: - `'label'`: the object name - `'bbox_2d'`: the object's bounding box coordinates as `[x1, y1, x2, y2]`. Respond in a **JSON array**, where each entry is a dictionary with `'label'` and `'bbox_2d'`.

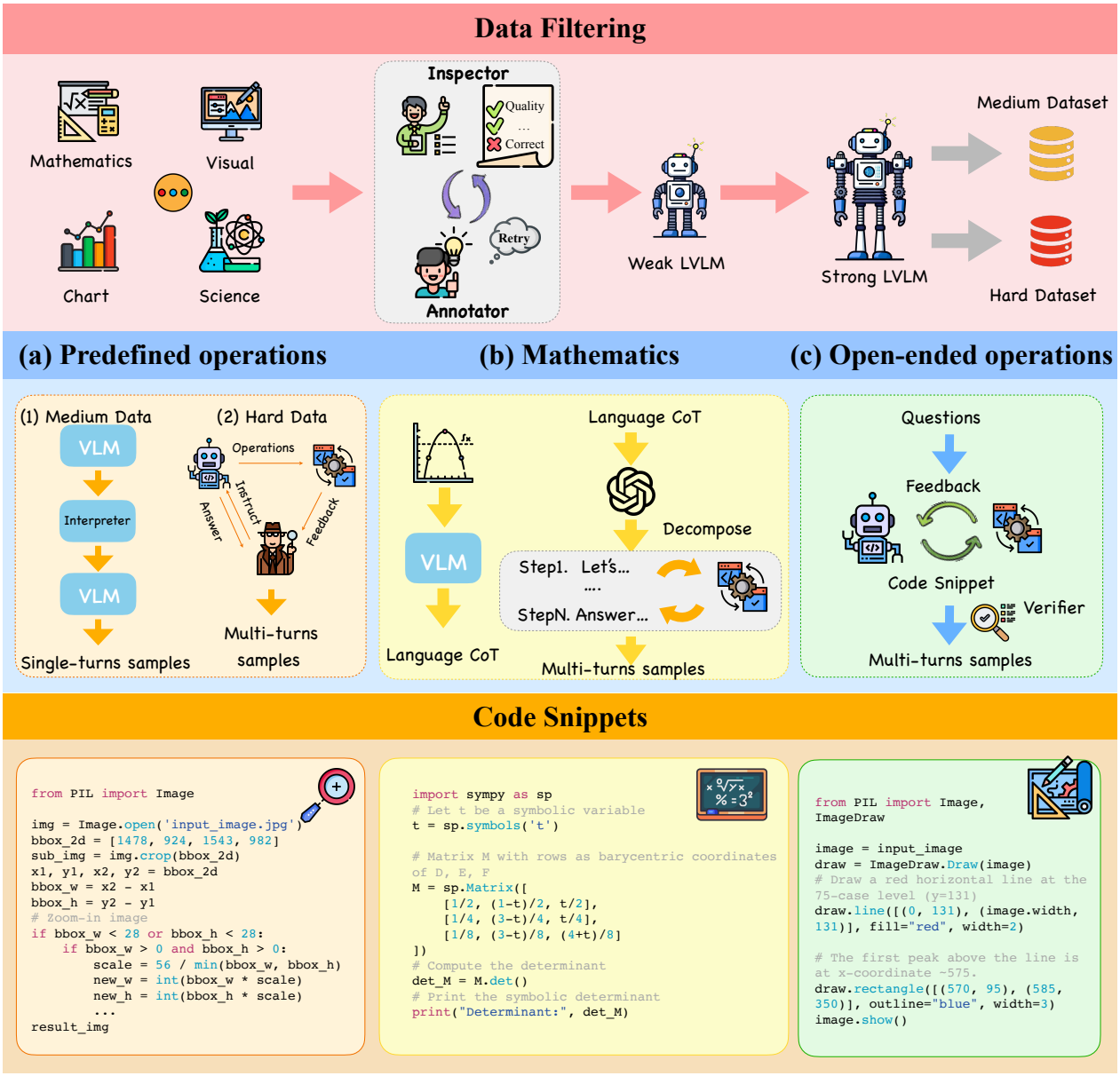


Figure 7. **Overview of the SFT dataset curation pipeline. Top**: Weak-to-strong filtering. Candidate samples from diverse domains (mathematics, science, visual reasoning, charts) are validated for quality and correctness through automated inspector modules. A weak VLM removes trivial or low-information cases, while a stronger VLM further stratifies the remaining data into medium- and hard-difficulty sets. **Middle**: Multi-turn atomic supervision. The curated data are organized into three categories. (a) Predefined image operations (e.g., crop, resize, rotate), where medium samples produce single-turn trajectories and hard samples produce multi-turn reasoning with interpreter feedback. (b) Mathematical reasoning, where language-based CoT traces are decomposed into step-level atomic operations and converted into executable code. (c) Open-ended visual operations (e.g., drawing, annotation), where questions, feedback, and snippet verification form multi-turn executable trajectories. **Bottom**: Example executable snippets illustrating the supervision format across image processing, symbolic computation, and visual annotation. **A detailed curation pipeline example is shown in Figure 8.**

8. Additional empirical studies

8.1. Visualization of sequence/turn-level rewards

Figure 6 illustrates how the sequence-level reward R_{seq} and the turn-level reward R_{turn} defined in the main paper are applied along a multi-turn trajectory in the persistent execution environment. Each query is solved through a sequence of *Reasoning–Code–Response* turns, where code is executed in a shared sandbox so that intermediate variables and visual artifacts can be reused across turns. After

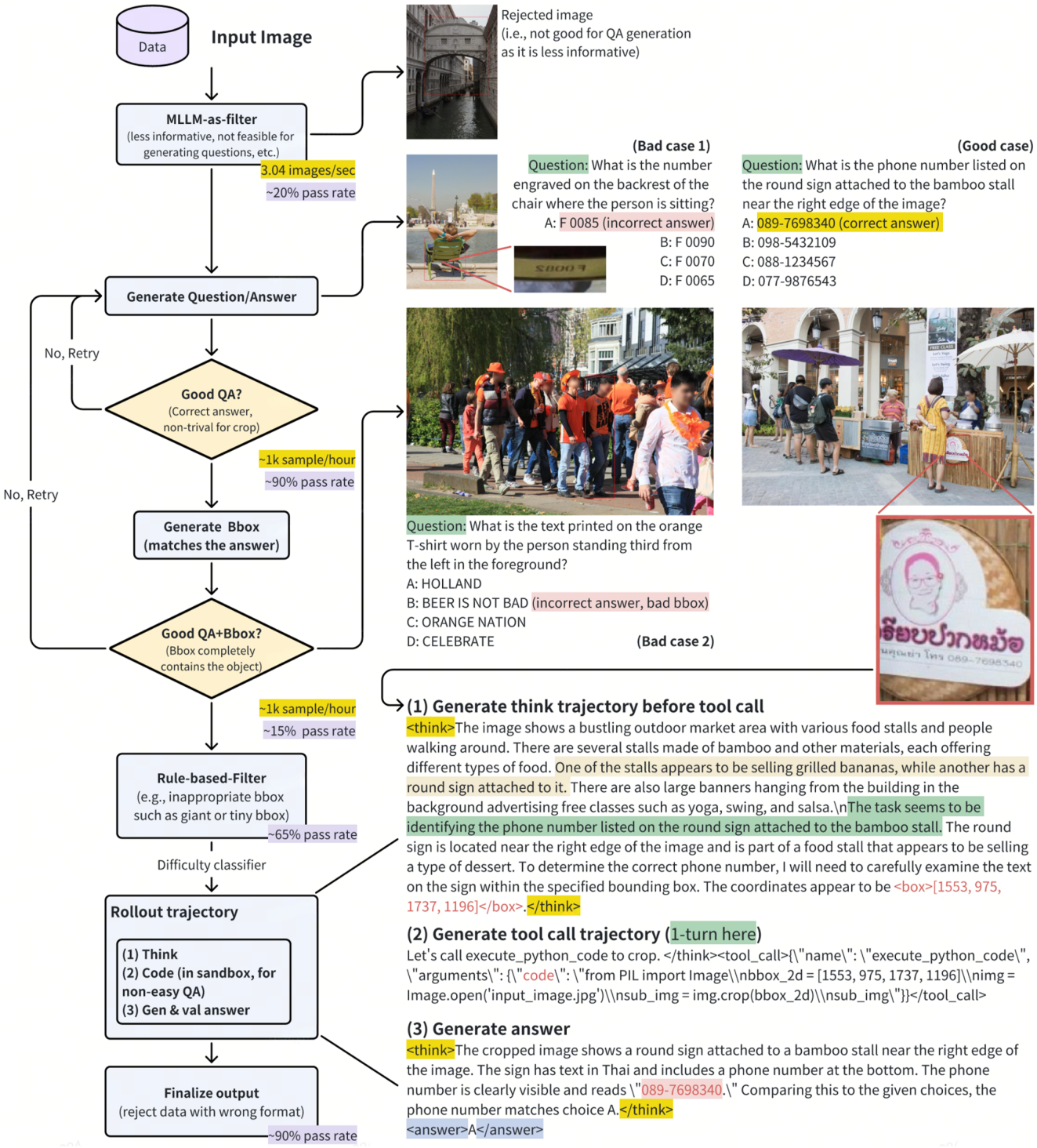


Figure 8. **An illustration of curating tool-integrated reasoning trajectories** (for cropping operations here). Representative good and bad cases are shown on the right, covering incorrect answers, trivial or mismatched bounding boxes, and fully valid QA pairs. A rule-based filter further removes outputs with implausible bounding boxes. Similar operations are applied when synthesizing other trajectories with different atomic capabilities. Best viewed in color with zooming in.

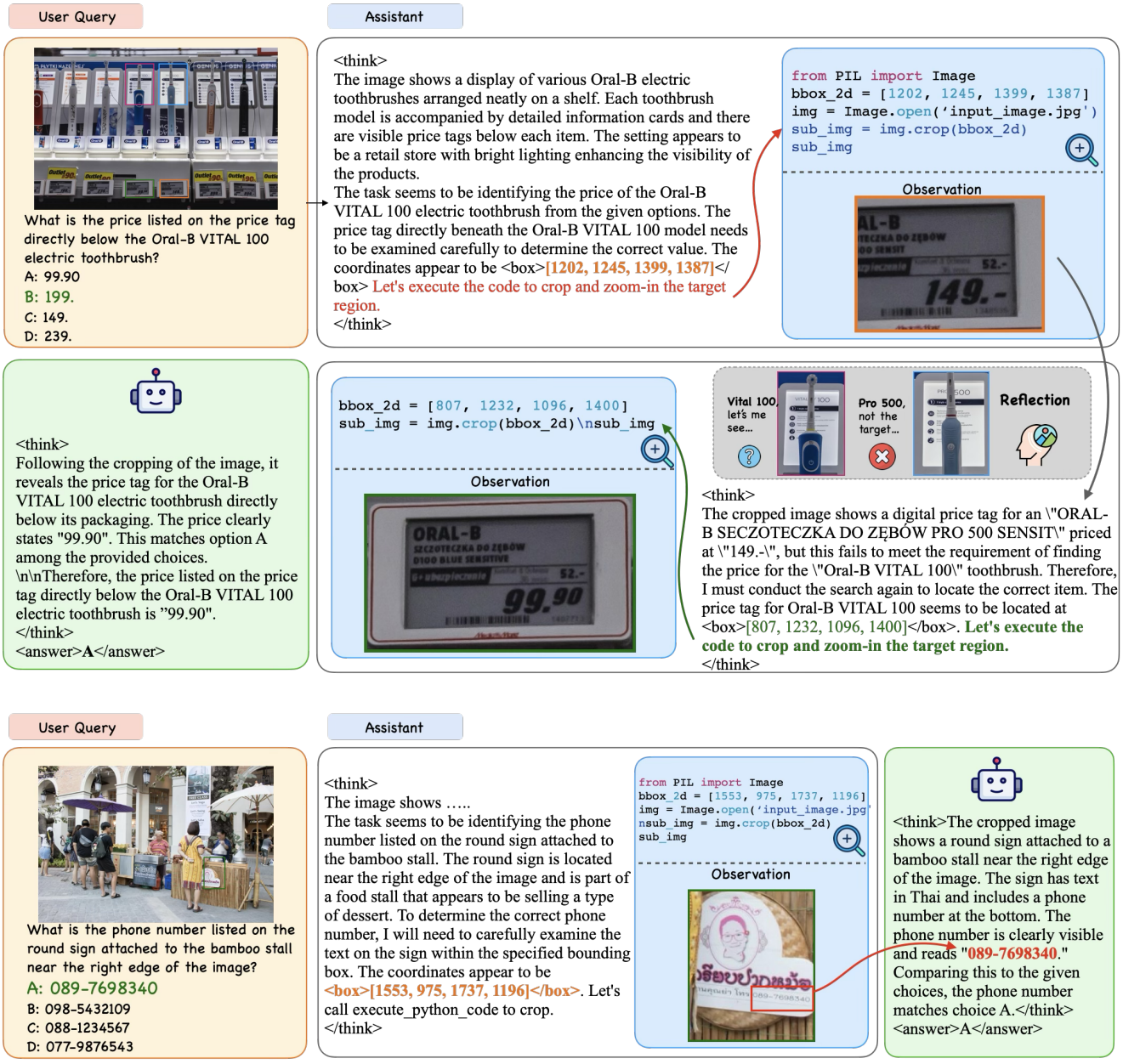


Figure 9. Example SFT training data of an atomic operation (`zoom-in` operation here). Top: two-turn, bottom: a single-turn trajectory.

the whole trajectory τ is completed, the sequence-level reward R_{seq} is computed from the final-answer correctness and the global tool-use statistics $(N_{\text{succ}}(\tau), N_{\text{total}}(\tau), \mu_{\text{acc}})$. The corresponding sequence-level advantage A_{seq} is then broadcast to all tokens in the trajectory (green bars at the bottom of the figure), providing an outcome-level learning signal that adaptively encourages or discourages overall tool usage depending on task difficulty.

Inside the red dashed box, the turn-level component is computed from execution outcomes at each turn m. Failed executions receive an immediate negative penalty $r_{\text{turn},m} < 0$, while successful or no-code turns receive $r_{\text{turn},m} = 0$. These per-turn penalties are accumulated into discounted returns G^m_{turn} and normalized into advantages A^m_{turn}, which are only assigned to the tokens of that specific turn (colored segments in the figure; hatched regions indicate zero turn-level signal). The final token-wise advantage is obtained by combining the global A_{seq} with the local A^m_{turn} of its turn.

Table 7. Prompt template for visual question validation.

You are a quality control assistant. Your task is to evaluate a visual question based on the provided image, question, and correct answer.

Image: [Image is attached]

Question: `{question}`

Provided Correct Answer: `{correct_answer}`

Evaluation Criteria:

1. **Correctness:** Is the provided "Correct Answer" truly the correct answer based on the image?

2. **Difficulty:** Is the question non-trivial? It should require careful observation of details and not be something overly simple or obvious (e.g., "What color is the sky?").

Your Response:

Respond with "GOOD" if the question meets BOTH criteria.

Respond with "BAD" if the question fails one or both criteria. Do not provide any other explanation or text.

Table 8. Prompt template for step-by-step solving with answer tag.

Solve the following problem step by step and then provide the final answer.

The final answer MUST BE enclosed within `<answer>` `</answer>` tags.

Question: `{question}`

8.2. Hyperparameters in our method

8.2.1. Sensitivity of R_{BAT} Hyperparameters

Recall that the sequence-level component of our reward is defined in Eq. (5) as

$$R_{\text{seq}}(\tau) = \Big(0.5 + 0.5 \cdot \mathbf{1}\{R_{\text{acc}}(\tau) > 0\}\Big)\, d(\mu_{\text{acc}})\, \frac{N_{\text{succ}}(\tau)}{N_{\text{total}}(\tau)}, \tag{5}$$

where the scaling term $d(\mu_{\text{acc}})$ is defined as $d(\mu_{\text{acc}}) = \sigma\big(\gamma(0.5 - \mu_{\text{acc}})\big) - \delta$, $\mu_{\text{acc}} \in [0, 1]$ is the group-level accuracy, $\sigma(z) = 1/(1+e^{-z})$ is the logistic function, and (γ, δ) control how strongly the group accuracy modulates the incentive on tool calls. Here, $\frac{N_{\text{succ}}(\tau)}{N_{\text{total}}(\tau)}$ measures the proportion of successful tool executions within the trajectory, and the leading term $\big(0.5+0.5\cdot\mathbf{1}\{R_{\text{acc}}(\tau) > 0\}\big)$ switches the base weight according to final-answer correctness. Intuitively, $d(\mu_{\text{acc}})$ decreases as μ_{acc} increases: it amplifies successful tool calls when the group is struggling (low μ_{acc}) and suppresses unnecessary calls when the group already performs well (high μ_{acc}). The hyperparameters control this behavior: γ adjusts how sharp the transition is, δ shifts the baseline and determines whether suppression occurs in high-accuracy regimes, and β is the discount factor for per-turn penalties in R_{turn}. In the main experiments we set $\gamma = 4$, $\delta = 0.2$, and $\beta = 0.2$. The sensitivity results are summarized in Figure 10.

8.2.2. Effective range and bounds of $d(\mu_{\text{acc}})$

As $\sigma(\cdot) \in (0, 1)$ for all real inputs and $\mu_{\text{acc}} \in [0, 1]$, the scaling term d is deterministically bounded as

$$-\delta < d(\mu_{\text{acc}}) < 1 - \delta.$$

Importantly, negative values of d are intentional rather than pathological: they occur only when the group-level accuracy μ_{acc} is sufficiently high and are used to discourage unnecessary tool calls on easy queries. The sign flip of d happens at a unique threshold

$$\mu^{\star}_{\text{acc}} = 0.5 - \frac{1}{\gamma}\,\sigma^{-1}(\delta), \quad \text{where } \sigma^{-1}(u) = \log\frac{u}{1-u}.$$

For $\gamma = 4$, $\delta = 0.2$, this gives a transition around

$$\mu^{\star}_{\text{acc}} \approx 0.5 + \frac{1}{4}\log\frac{1-0.2}{0.2},$$

i.e., only when most rollouts in the group are already correct does d become slightly negative. In all other regimes (medium or low μ_{acc}), $d > 0$ and R_{BAT} increases the relative value of successful tool calls. Together with the per-turn penalty R_{turn} for failed execution, this design prevents degenerate tool-spamming or tool-off behaviors: on easy tasks, negative d discourages extra calls; on hard tasks, positive d amplifies the benefit of correctly executed tools.

8.2.3. Hyperparameter over (γ, δ)

We run an ablation on (γ, δ) to probe R_{BAT}'s behavior in practice. Concretely, we train three settings, $(4, 0.2)$, $(4, 0.0)$ and $(5, 0.2)$, and monitor training accuracy and average tool calls per example. This lets us (i) compare $\gamma \in 4, 5$ at fixed $\delta = 0.2$, and (ii) isolate the effect of enabling vs. disabling suppression at high group-level accuracy by varying $\delta \in 0, 0.2$ at fixed $\gamma = 4$.

Empirically, γ has little effect on training accuracy, while setting $\delta = 0$ removes suppression for high-μ_{acc} groups and causes substantially more tool calls with similar accuracy, i.e., tool overuse. Our choice $(4, 0.2)$ keeps accuracy high while restraining unnecessary tool usage. The result is shown as Figure 10.

8.3. Analysis of Reasoning Depth

Our policy aligns reasoning depth with task difficulty. We plot *task difficulty* (measured by GPT-4o ACC.) vs. *number of turns* (see Fig. 11) and validate that harder problems indeed induce longer reasoning turns, while easier ones terminate early.

Table 9. Prompt template for revised thinking with code interpreter.

You are a helpful AI assistant. Initially, when solving a question, you would need to think step by step, without the ability to use code for calculation. Now, you have the capability to write code to use the code interpreter for calculation. The code will be executed by a sandbox, and the result can be returned to enhance your reasoning process. You can now leverage code to enhance your calculation while still maintaining the reasoning process.

The thinking process can have multiple code snippets. Each code snippet is wrapped with

```
<code>
```python
code snippet
```
</code>
```

The returned result is wrapped with

```
<interpreter> execution results</interpreter>
```

Goal: Modify the original thinking process to make it more accurate by replacing manual calculation steps that can benefit from code execution with the corresponding code snippets and their interpreter's execution results. The core reasoning logic from the original thinking process, including any unsuccessful attempts, should remain unchanged. You should only replace the necessary manual calculation steps with code and interpreter's execution results, without altering the rest tokens of the thinking process.

User Question: `{question}`

Original Thinking Process (without code interpreter's support):

`<original_thinking_process>` `{original_response}` `</original_thinking_process>`

Details:

1. Identify sections where code execution could speed up the reasoning process or make the calculation more accurate. For simple calculations, you should keep the original text-based reasoning process without executing any code.

2. Replace the manual calculation steps with code snippets and the corresponding interpreter's execution results.

3. Keep the logical flow of the reasoning process intact, including any failed exploration attempts that were part of the initial process.

4. The code snippets should be complete scripts, including necessary imports.

5. Outputs in the code snippets must explicitly call the **print** function.

6. Execution results should match the model's output exactly, with no extra or missing tokens.

7. If, during the revised thinking process, you obtain the same result as in the original reasoning, you may omit numerical computations and refrain from simplifying to specific numeric values.

8. If the Original Thinking Process does not include an `<answer>` section at the end, please add it: `<answer> \boxed{{'The final answer goes here.'}} </answer>`

Revised Thinking Process (With code interpreter's support):

9. Additional qualitative results

Reward-hacking case when using naive tool call reward for code generation. A naive reward scheme that simply reinforces every successful tool call is prone to reward hacking, where the model exploits loopholes in the reward design rather than genuinely improving reasoning. For instance, we observe failure cases in Figure 12 in which the model generates degenerate tool outputs (e.g., code consisting only of commentary lines without actual execution) that nevertheless satisfy superficial reward signals. Such behaviors artificially inflate tool success metrics while providing no real contribution to solving the task, thereby misleading training and undermining reasoning quality.

Table 10. Prompt template for Reinforcement Learning Rollout.

User. <image> Question: {question}

Think step-by-step within <think></think>. You now have the ability to selectively write executable Python code to enhance your reasoning process. The Python code should be complete scripts, including necessary imports.

Each code snippet is wrapped with

<code>
```python
code snippet
```
</code>

You must provide your final answer in <answer> </answer>.

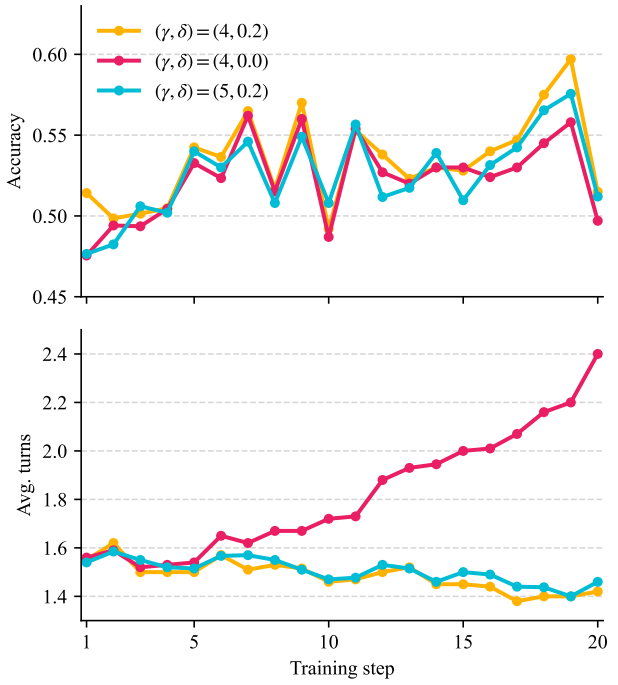


Figure 10. Training dynamics of R_{BAT} under three (γ, δ) configurations. We plot accuracy (top) and average reasoning turns (bottom) over training steps on the union of RL benchmarks. Accuracy is relatively stable across $\gamma \in \{4, 5\}$ (i.e., γ mainly smooths the transition in $d(\mu_{\text{acc}})$), whereas setting $\delta = 0$ removes suppression for high-μ_{acc} groups and leads to steadily increasing tool usage with only marginal accuracy gains. Our default $(\gamma, \delta) = (4, 0.2)$ maintains high accuracy while restraining unnecessary tool calls.

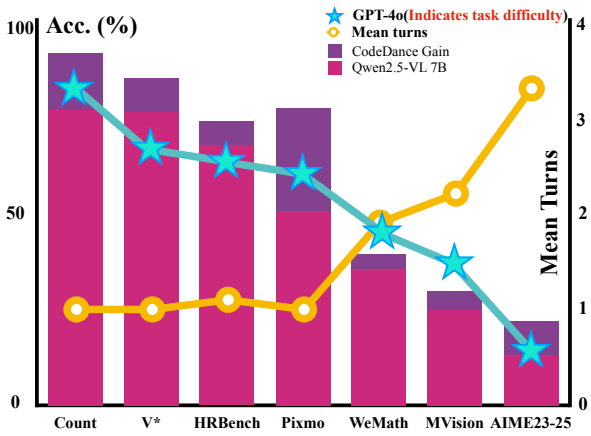


Figure 11. Reasoning depth vs. task difficulty.

9.1. Failure cases observed in our experiments

Although our model performs competitively across benchmarks, several failure modes are still observed, and we summarize them in Figure 13.

First, inaccurate or suboptimal cropping may occur when the model misidentifies the target region or when visual cues are subtle. **As shown in Case A**, the model selects an overly large bounding box around the person, causing the cropped image to mix multiple objects; the model still answers correctly, but the tool invocation is clearly misaligned. Second, the model may miss partially obscured objects in complex scenes. **In Case B**, our model correctly identifies and marks visible individuals but fails to consider whether additional people might be hidden or partially occluded, leading to an incomplete final count.

These cases highlight the remaining challenges in precise localization and robust multi-step verification under ambiguous or cluttered visual conditions.

9.2. Additional novel reasoning trajectories

In Figure 14, we show step-by-step reasoning trajectories across three distinct vision tasks on tool transfer:

Figure 14 (Top): The assistant tackles a spatial relational question by first localizing both the bear and the white rock using bounding boxes. It then uses PIL to draw red/blue rectangles around each object, visually verifying their relative positions. This demonstrates code-mediated spatial reasoning. Instead of relying on implicit attention maps or pretrained spatial priors, the model actively constructs visual evidence through code. The act of drawing bounding boxes serves as an internal "visual scratchpad", enabling explicit comparison of object positions, which is crucial for fine-grained spatial inference where ambiguity exists.

Figure 14 (Mid): The assistant identifies four candidate regions containing parrots based on initial visual inspection.

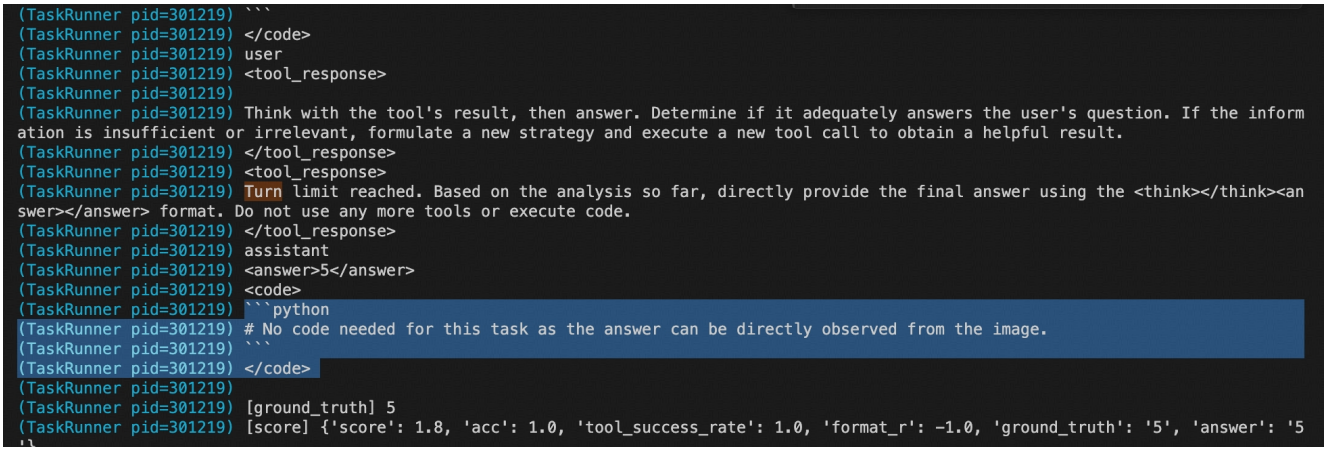


Figure 12. An example of a reasoning trajectory exhibiting reward hacking (using a DeepEyes-style tool reward for code generation). The MLLM exploits the reward by generating code with only commentary lines, which is not actually executed.

It then executes a loop of `img.crop(bounding box)` operations to isolate each region, visually confirming that each cropped area contains a unique, clearly distinguishable parrot. This iterative cropping and verification ensures no over- or under-counting. This exemplifies verification-driven counting. Rather than predicting a number directly (which risks hallucination or confusion with similar objects), the system uses tool-based segmentation to reduce the problem to a series of binary verifications ("Is this one a parrot?"). The modularity of PIL operations allows the model to treat counting as a compositional task — scaling naturally to more complex scenes.

Figure 14 (Bottom): Given a scientific graph with brightness vs. time, the assistant zooms into panel (c) using `img.crop()` to focus on the region with arrows. It observes sharp downward spikes in the curve at those points and infers they represent sudden drops in brightness, not measurement noise or calibration artifacts — based on the magnitude and shape of the dips.

Similarly, the trajectories in Figure 15 reveal iterative, self-correcting reasoning enabled by dynamic tool composition, which is based on tool transfer ability since we only define a single set of tool/ability for each task during SFT.

Top-row of Figure 15: The assistant first attempts to locate the person in the striped shirt relative to the woman drinking. It initially misidentifies coordinates, so it composes two tools: First, it uses `cv2.circle()` to draw red points at hypothesized locations — visually flagging potential errors. Then, it corrects the coordinates and uses `PIL.Image.crop()` to zoom into the region for closer inspection. Finally, it confirms the spatial relationship: the striped-shirt person is indeed to the left, seated next to the drinking woman — no occlusion or misleading posture.

Bottom-row of Figure 15: The assistant must extract a precise numerical value from a scientific plot showing (Δm^2) vs. $sin^2(2\theta)$. It follows a multi-step strategy: Identify region: Uses `ImageDraw.rectangle()` to highlight the blue shaded 90% confidence level (CL) band. Zoom in: Crops the upper boundary of this region using `PIL.Image.crop()` to isolate the extreme right edge — where (Δm^2) reaches its maximum within the CL. Finally interpret scale and answer.

While these reasoning trajectories during RL exploration are not without flaws, e.g. occasionally exhibiting imprecise coordinate estimation or redundant tool calls, they collectively demonstrate the potential of tool-augmented multimodal reasoning.

10. Discussion

Why code-based tool use, rather than API-style calls? We adopt Python code as the medium for tool use because it provides a general and compositional interface. Unlike fixed API schemas, code naturally supports both tool invocation and program logic (e.g., sequencing, conditionals, loops, numerical computation). This richer interface allows models to flexibly define and combine operations, and it produces transparent and verifiable execution traces that can be systematically inspected. In practice, code also makes extension straightforward: adding a new tool only requires exposing its API, without redesigning templates, retraining connectors, or engineering complex prompts.

Why a single dense model, rather than an agent pipeline? A unified dense model offers several practical advantages over modular agent workflows: (1) it avoids error propagation across multiple components by learning an end-to-end interface; (2) it achieves lower latency and compute cost, since reasoning and tool orchestration are handled in a single forward pass; (3) it is more robust, as performance does not hinge on the reliability of each submodule; and (4) it benefits from a unified optimization tar-

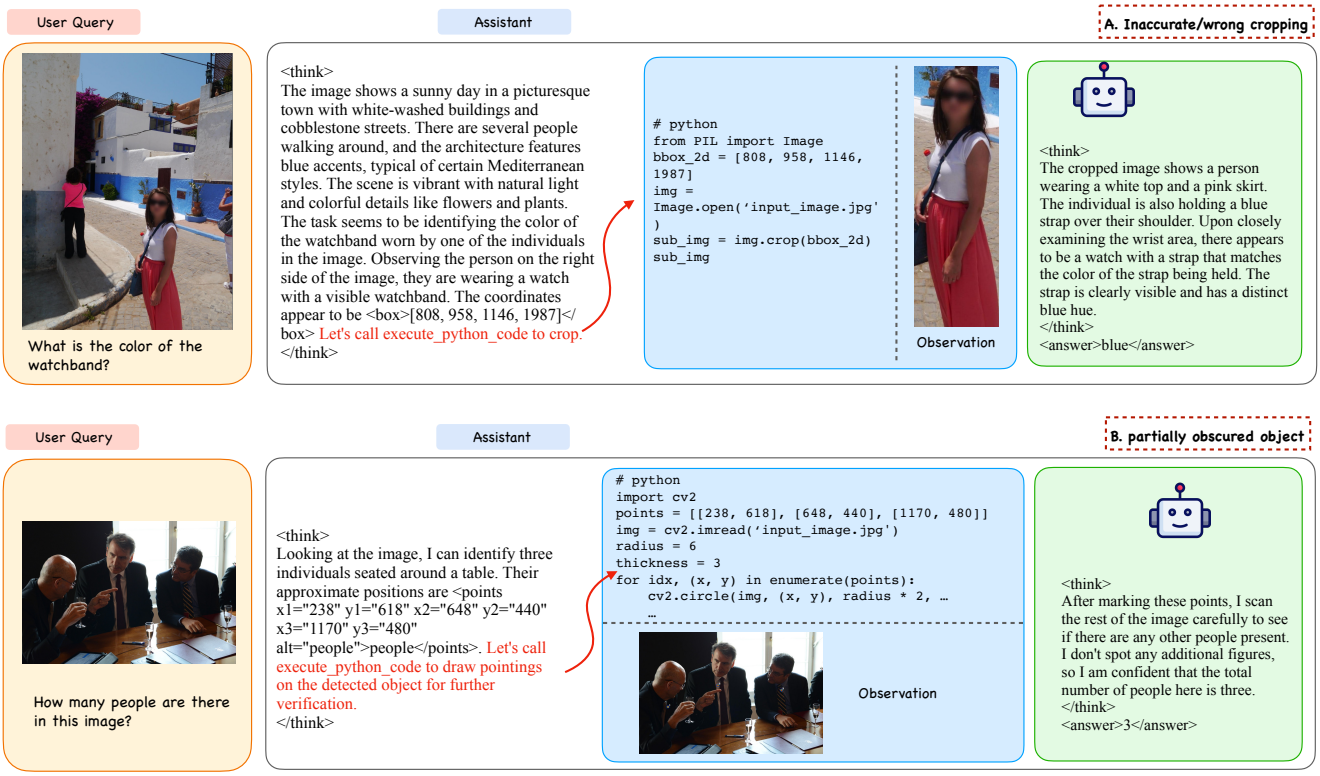


Figure 13. Failure cases found in our empirical studies. **A:** The model performs wrongly cropping. **B:** The person on the right edge is partially obscured, thus hard to count.

get, whereas agent systems often require additional policies or connectors to be separately tuned.

In addition, given realistic compute constraints, most of our experiments in this work are conducted with 7B-scale models (e.g., Qwen-2.5-VL-7B), where we already observe promising effects: consistent gains across general understanding and complex reasoning benchmarks, and the emergence of new behaviors (e.g., novel tool use and tool compositions of atomic skills to new tasks). These empirical observations *are easier to scale* within a single dense model, while agent pipelines introduce many interacting modules that complicate both training and deployment. Overall, our design favors simplicity, efficiency, and scalability, making it a more practical foundation for future progress.

11. Broader impact

This work contributes toward building more transparent and verifiable multimodal reasoning systems by adopting executable code as the unified medium for tool use. The ability to generate interpretable traces and intermediate artifacts can benefit applications where accountability and auditability are essential, such as scientific analysis and education. At the same time, code-generating models pose risks: malicious users could potentially exploit them for unsafe automation, and generated visual artifacts might be misused to mislead or manipulate. To mitigate these concerns, we recommend pairing such systems with appropriate safeguards, including safety filters, usage constraints, and responsible deployment practices. By doing so, the benefits of executable visual reasoning can be realized while minimizing the potential for misuse.

12. Limitations and future work

Limitations. While our method demonstrates promising emergent behaviors and strong performance across diverse visual reasoning tasks, several limitations remain. First, the reliance on high-quality synthetic trajectories implies that certain real-world reasoning patterns may be underrepresented, potentially limiting robustness in open-domain scenarios. Second, although code provides a general interface, extending to richer modalities (e.g., audio) or domain-specific tools (e.g., medical applications) will require additional engineering. Finally, due to compute constraints, our evaluations are primarily conducted on 7B-scale models; the scalability of emergent behaviors at larger scales remains to be systematically examined. Nevertheless, our preliminary experiments suggest a promising trend when scaling up model capacity and compute resources.

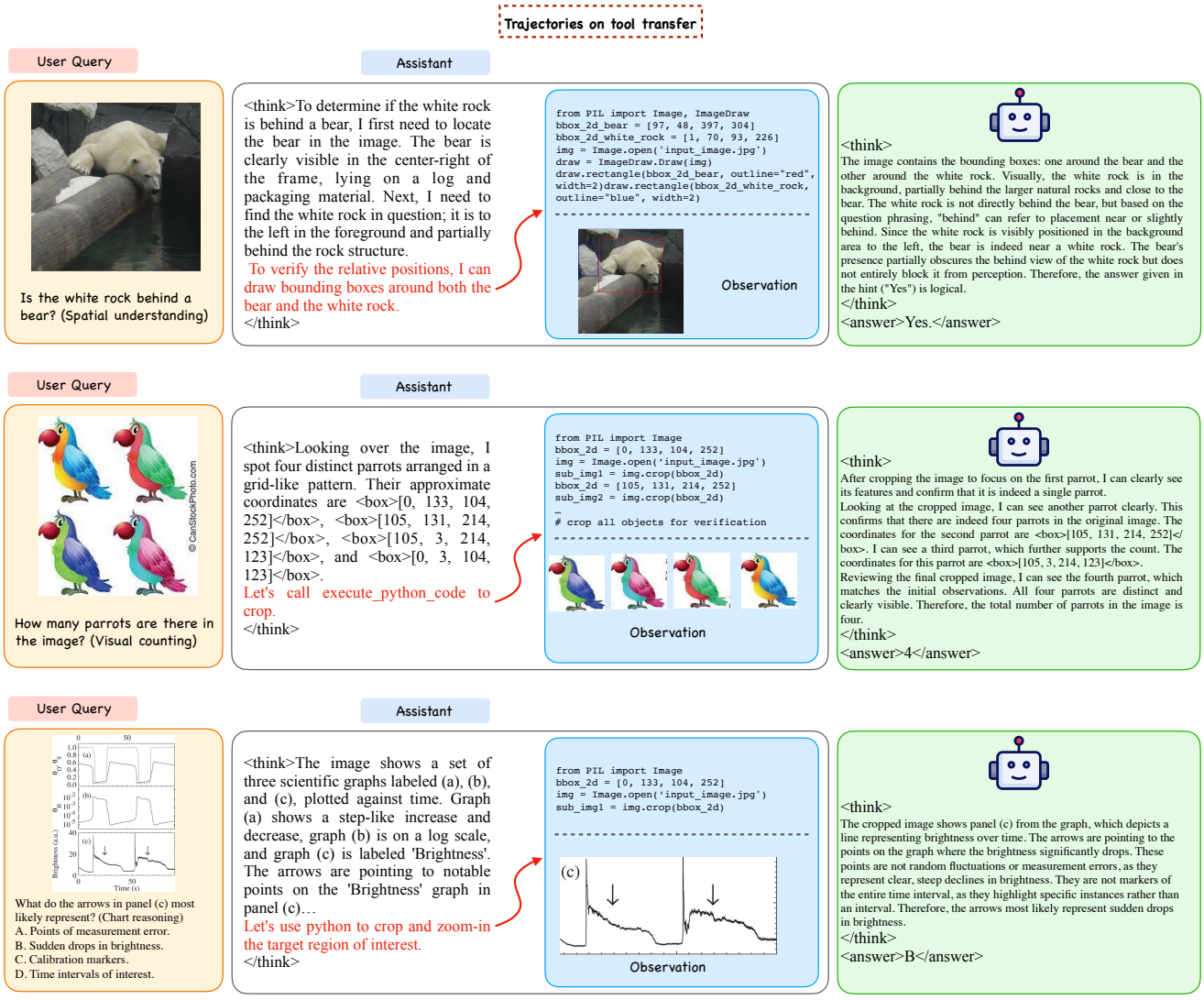


Figure 14. Novel reasoning trajectories on tool transfer to other tasks.

Trajectories on tools composition

User Query



Is the striped shirt to the left of the woman drinking?

Assistant

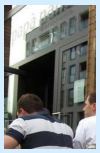
<think>
I see the striped shirt is indeed to the left of the woman drinking, but I overlooked the coordinates slightly. Let's call execute_python_code to draw pointings on the detected object for further verification.
</think>

```
# draw points
import cv2
points = [[51, 247], [329, 211]]
img = cv2.imread('input_image.jpg')
radius = 6
cv2.circle(img, (x, y), radius * 2, (255, 0, 0), -1)
cv2.putText(img, str(idx+1), (x + radius + 3, ...)
img
```



Observation

<think>
After cropping, it's clear from the cropped image that the person wearing a striped shirt is to the left of the woman seen here drinking. The cropped area shows the shoulder and arm of the individual in the striped shirt, positioned to the left of the arm of the woman who seems to be in the act of drinking. There is no indication of any obstruction or misalignment that would suggest otherwise. Therefore, the detection is correct.
</think>
<answer>Yes.</answer>

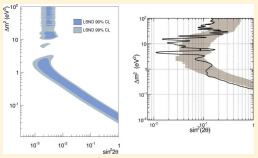


Observation

```
# crop
from PIL import Image
img = Image.open('input_image.jpg')
bbox_2d = [51, 0, 235, 298]
sub_img = img.crop(bbox_2d)
```

<think>
Now that I've redone the detection with improved coordinates given by the hint, the striped shirt seems to be correctly positioned relative to the woman drinking. The woman in green appears on the far left among the patrons, while the person in a striped shirt is seated next to her.
Let's call execute_python_code to crop.
</think>

User Query

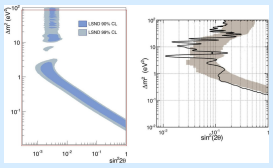


What is the highest value of (\Delta m^2) (in (eV^2)) that is within the 90% confidence level (CL) according to the LSND data shown in the figure?
A. (10^{-1} eV^2) B. (10^2 eV^2)
C. (10^1 eV^2) D. (10^0 eV^2)

Assistant

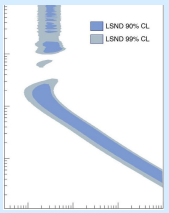
<think>
To solve this problem, we need to analyze the left figure of the provided image, which shows the (\Delta m^2) (in (eV^2)) versus (\sin^2 2\theta) (in logarithmic scale). The question asks for the highest value of (\Delta m^2) at the 90% confidence level (CL) according to the LSND data.
1. Identify the relevant region: The legend on the left figure indicates that the 90% CL confidence level is represented by the blue shaded area.
2. Locate the highest region of the 90% CL band: Looking at the blue shaded area, we can see that as the (\sin^2 2\theta) value decreases (i.e., moves to the right on the plot), the permissible range of (\Delta m^2) increases. The highest point, or the upper limit, of this permissible range is the most interesting for answering the question.
3. Estimate the value from the plot: We need to estimate the value of (\Delta m^2) (on the vertical axis) that corresponds to the extreme right of the blue band. This requires a more precise measurement than can be done just by looking at the figure.
</think>

```
# draw bbox to highlight
from PIL import Image, ImageDraw
bbox_2d = [133, 37, 933, 1073]
img = Image.open('input_image.jpg')
draw = ImageDraw.Draw(img)
draw.rectangle(bbox_2d, outline="red", width=2)
```



Observation

<think>
The cropped image provides a closer view of the blue shaded region labeled "LSND 90% CL." The left figure shows the data with logarithmic scales on both axes. The task is to find the highest value of (\Delta m^2) that is within this 90% confidence level band.
1....2....
3. Estimate the value from the axis: The top of the blue band is clearly above the value of (10^0) (which is 1) on the y-axis. It is also below the value of (10^1) (which is 10) on the y-axis. Therefore, the highest value is greater than 1 and less than 10 (eV^2).
Looking at the options, the value (10^1 eV^2) is the most accurate description of the highest value within the given range.
</think>
<answer>\boxed{C. (10^1 eV^2)}</answer>



Observation

```
# crop
from PIL import Image
img =
Image.open('input_image.
jpg')
bbox_2d = [133, 37, 933,
1073]
sub_img =
img.crop(bbox_2d)
```

<think>
The red box drawn on the left image highlights the upper boundary of the 90% confidence level (CL) region for (\Delta m^2) as a function of (\sin^2 2\theta). By examining this box, we can estimate the highest value of (\Delta m^2) within this region. From the logarithmic scale on the y-axis, the upper boundary of the red box corresponds to a value of (\Delta m^2) that is just below the 10(^1) (10) line, but clearly above the 10(^0) (1) line. This corresponds to a value of approximately (10^1 eV^2).
Let's call execute_python_code to crop.
</think>

Figure 15. Reasoning trajectories on tools composition.

Future Work. Our framework demonstrates the potential of multimodal reasoning models to support natural conversations with seamless and proactive tool use through executable code, thereby enabling more advanced problem-solving capabilities. Looking ahead, we envision that the ability to "think with images" will evolve beyond the vision modality and fixed schemas, fostering novel tool discovery and the spontaneous composition of tools in a more generalized and efficient manner. Such directions may ultimately pave the way toward multimodal agents that are both versatile and adaptive across diverse domains.

References

[1] Jinze Bai, Shuai Bai, Shusheng Yang, Shijie Wang, Sinan Tan, Peng Wang, Junyang Lin, Chang Zhou, and Jingren Zhou. Qwen-vl: A versatile vision-language model for understanding, localization, text reading, and beyond. *arXiv preprint arXiv:2308.12966*, 2023. 6

[2] Shuai Bai, Keqin Chen, Xuejing Liu, Jialin Wang, Wenbin Ge, Sibo Song, Kai Dang, Peng Wang, Shijie Wang, Jun Tang, Humen Zhong, Yuanzhi Zhu, Mingkun Yang, Zhaohai Li, Jianqiang Wan, Pengfei Wang, Wei Ding, Zheren Fu, Yiheng Xu, Jiabo Ye, Xi Zhang, Tianbao Xie, Zesen Cheng, Hang Zhang, Zhibo Yang, Haiyang Xu, and Junyang Lin. Qwen2.5-vl technical report. *arXiv preprint arXiv:2502.13923*, 2025. 9

[3] Tom Brown, Benjamin Mann, Nick Ryder, Melanie Subbiah, Jared D Kaplan, Prafulla Dhariwal, Arvind Neelakantan, Pranav Shyam, Girish Sastry, Amanda Askell, et al. Language models are few-shot learners. *Advances in neural information processing systems*, 33:1877–1901, 2020. 2

[4] Lin Chen, Jinsong Li, Xiaoyi Dong, Pan Zhang, Conghui He, Jiaqi Wang, Feng Zhao, and Dahua Lin. Sharegpt4v: Improving large multi-modal models with better captions. In *European Conference on Computer Vision*, pages 370–387. Springer, 2024. 10

[5] Xinyan Chen, Renrui Zhang, Dongzhi Jiang, Aojun Zhou, Shilin Yan, Weifeng Lin, and Hongsheng Li. Mint-cot: Enabling interleaved visual tokens in mathematical chain-of-thought reasoning. *arXiv preprint arXiv:2506.05331*, 2025. 4, 10

[6] Jiwan Chung, Junhyeok Kim, Siyeol Kim, Jaeyoung Lee, Min Soo Kim, and Youngjae Yu. Don't look only once: Towards multimodal interactive reasoning with selective visual revisitation. *arXiv preprint arXiv:2505.18842*, 2025. 2

[7] Wenliang Dai, Junnan Li, Dongxu Li, Anthony Tiong, Junqi Zhao, Weisheng Wang, Boyang Li, Pascale N Fung, and Steven Hoi. Instructblip: Towards general-purpose vision-language models with instruction tuning. *Advances in neural information processing systems*, 36:49250–49267, 2023. 10

[8] Matt Deitke, Christopher Clark, Sangho Lee, Rohun Tripathi, Yue Yang, Jae Sung Park, Mohammadreza Salehi, Niklas Muennighoff, Kyle Lo, Luca Soldaini, et al. Molmo and pixmo: Open weights and open data for state-of-the-art vision-language models. In *Proceedings of the Computer Vision and Pattern Recognition Conference*, pages 91–104, 2025. 6, 11

[9] Haodong Duan, Junming Yang, Yuxuan Qiao, Xinyu Fang, Lin Chen, Yuan Liu, Xiaoyi Dong, Yuhang Zang, Pan Zhang, Jiaqi Wang, et al. Vlmevalkit: An open-source toolkit for evaluating large multi-modality models. In *Proceedings of the 32nd ACM international conference on multimedia*, pages 11198–11201, 2024. 6

[10] Jiazhan Feng, Shijue Huang, Xingwei Qu, Ge Zhang, Yujia Qin, Baoquan Zhong, Chengquan Jiang, Jinxin Chi, and Wanjun Zhong. Retool: Reinforcement learning for strategic tool use in llms. *arXiv preprint arXiv:2504.11536*, 2025. 2, 10, 11

[11] Wei Fu, Jiaxuan Gao, Xujie Shen, Chen Zhu, Zhiyu Mei, Chuyi He, Shusheng Xu, Guo Wei, Jun Mei, Jiashu Wang, et al. Areal: A large-scale asynchronous reinforcement learning system for language reasoning. *arXiv preprint arXiv:2505.24298*, 2025. 10

[12] Jiahui Gao, Renjie Pi, Jipeng Zhang, Jiacheng Ye, Wanjun Zhong, Yufei Wang, Lanqing Hong, Jianhua Han, Hang Xu, Zhenguo Li, et al. G-llava: Solving geometric problem with multi-modal large language model. *arXiv preprint arXiv:2312.11370*, 2023. 10

[13] Alexander Kirillov, Eric Mintun, Nikhila Ravi, Hanzi Mao, Chloe Rolland, Laura Gustafson, Tete Xiao, Spencer Whitehead, Alexander C Berg, Wan-Yen Lo, et al. Segment anything. In *Proceedings of the IEEE/CVF international conference on computer vision*, pages 4015–4026, 2023. 11

[14] Jongwoo Ko, Sungnyun Kim, Sungwoo Cho, and Se-Young Yun. Flex-judge: Think once, judge anywhere. *arXiv preprint arXiv:2505.18601*, 2025. 2

[15] Woosuk Kwon, Zhuohan Li, Siyuan Zhuang, Ying Sheng, Lianmin Zheng, Cody Hao Yu, Joseph E. Gonzalez, Hao Zhang, and Ion Stoica. Efficient memory management for large language model serving with pagedattention. In *Proceedings of the ACM SIGOPS 29th Symposium on Operating Systems Principles*, 2023. 9

[16] Mengcheng Lan, Chaofeng Chen, Yue Zhou, Jiaxing Xu, Yiping Ke, Xinjiang Wang, Litong Feng, and Wayne Zhang. Text4seg: Reimagining image segmentation as text generation. *arXiv preprint arXiv:2410.09855*, 2024. 10

[17] Qianlong Li, Chen Huang, Shuai Li, Yuanxin Xiang, Deng Xiong, and Wenqiang Lei. Graphotter: Evolving llm-based graph reasoning for complex table question answering. *arXiv preprint arXiv:2412.01230*, 2024. 4

[18] Pan Lu, Hritik Bansal, Tony Xia, Jiacheng Liu, Chunyuan Li, Hannaneh Hajishirzi, Hao Cheng, Kai-Wei Chang, Michel Galley, and Jianfeng Gao. Mathvista: Evaluating mathematical reasoning of foundation models in visual contexts. *arXiv preprint arXiv:2310.02255*, 2023. 6

[19] Ahmed Masry, Do Xuan Long, Jia Qing Tan, Shafiq Joty, and Enamul Hoque. Chartqa: A benchmark for question answering about charts with visual and logical reasoning. *arXiv preprint arXiv:2203.10244*, 2022. 6

[20] Ahmed Masry, Megh Thakkar, Aayush Bajaj, Aaryaman Kartha, Enamul Hoque, and Shafiq Joty. Chartgemma: Visual instruction-tuning for chart reasoning in the wild. *arXiv preprint arXiv:2407.04172*, 2024. 11

[21] Ahmed Masry, Mohammed Saidul Islam, Mahir Ahmed, Aayush Bajaj, Firoz Kabir, Aaryaman Kartha, Md Tahmid Rahman Laskar, Mizanur Rahman, Shadikur Rahman, Mehrad Shahmohammadi, et al. Chartqapro: A more diverse and challenging benchmark for chart question answering. *arXiv preprint arXiv:2504.05506*, 2025. 11

[22] Fanqing Meng, Lingxiao Du, Zongkai Liu, Zhixiang Zhou, Quanfeng Lu, Daocheng Fu, Tiancheng Han, Botian Shi, Wenhai Wang, Junjun He, et al. Mm-eureka: Exploring the frontiers of multimodal reasoning with rule-based reinforcement learning. *arXiv preprint arXiv:2503.07365*, 2025. 11

[23] OpenAI. Openai o3 and o4-mini system card. https://cdn.openai.com/pdf/2221c875-02dc-

4789-800b-e7758f3722c1/o3-and-o4-mini-system-card.pdf, 2025. System Card. 2, 4, 11

[24] Roni Paiss, Ariel Ephrat, Omer Tov, Shiran Zada, Inbar Mosseri, Michal Irani, and Tali Dekel. Teaching CLIP to Count to Ten. *arXiv preprint arXiv:2302.12066*, 2023. 6

[25] Runqi Qiao, Qiuna Tan, Guanting Dong, Minhui Wu, Chong Sun, Xiaoshuai Song, Zhuoma GongQue, Shanglin Lei, Zhe Wei, Miaoxuan Zhang, et al. We-math: Does your large multimodal model achieve human-like mathematical reasoning? *arXiv preprint arXiv:2407.01284*, 2024. 6

[26] Timo Schick, Jane Dwivedi-Yu, Roberto Dessì, Roberta Raileanu, Maria Lomeli, Eric Hambro, Luke Zettlemoyer, Nicola Cancedda, and Thomas Scialom. Toolformer: Language models can teach themselves to use tools. *Advances in Neural Information Processing Systems*, 36:68539–68551, 2023. 4

[27] John Schulman, Filip Wolski, Prafulla Dhariwal, Alec Radford, and Oleg Klimov. Proximal policy optimization algorithms. *arXiv preprint arXiv:1707.06347*, 2017. 10

[28] Zhihong Shao, Peiyi Wang, Qihao Zhu, Runxin Xu, Junxiao Song, Xiao Bi, Haowei Zhang, Mingchuan Zhang, YK Li, Yang Wu, et al. Deepseekmath: Pushing the limits of mathematical reasoning in open language models. *arXiv preprint arXiv:2402.03300*, 2024. 4, 10

[29] Yongliang Shen, Kaitao Song, Xu Tan, Dongsheng Li, Weiming Lu, and Yueting Zhuang. Hugginggpt: Solving ai tasks with chatgpt and its friends in hugging face. *Advances in Neural Information Processing Systems*, 36:38154–38180, 2023. 4

[30] Guangming Sheng, Chi Zhang, Zilingfeng Ye, Xibin Wu, Wang Zhang, Ru Zhang, Yanghua Peng, Haibin Lin, and Chuan Wu. Hybridflow: A flexible and efficient rlhf framework. *arXiv preprint arXiv: 2409.19256*, 2024. 6

[31] Vaishnavi Shrivastava, Ahmed Awadallah, Vidhisha Balachandran, Shivam Garg, Harkirat Behl, and Dimitris Papailiopoulos. Sample more to think less: Group filtered policy optimization for concise reasoning. *arXiv preprint arXiv:2508.09726*, 2025. 4

[32] Alex Su, Haozhe Wang, Weiming Ren, Fangzhen Lin, and Wenhu Chen. Pixel reasoner: Incentivizing pixel-space reasoning with curiosity-driven reinforcement learning. *arXiv preprint arXiv:2505.15966*, 2025. 2, 4, 10, 11

[33] Zhaochen Su, Linjie Li, Mingyang Song, Yunzhuo Hao, Zhengyuan Yang, Jun Zhang, Guanjie Chen, Jiawei Gu, Juntao Li, Xiaoye Qu, et al. Openthinkimg: Learning to think with images via visual tool reinforcement learning. *arXiv preprint arXiv:2505.08617*, 2025. 2

[34] Dídac Surís, Sachit Menon, and Carl Vondrick. Vipergpt: Visual inference via python execution for reasoning. In *Proceedings of the IEEE/CVF international conference on computer vision*, pages 11888–11898, 2023. 4

[35] Xu Wan, Wei Wang, Wenyue Xu, Wotao Yin, Jie Song, and Mingyang Sun. Adapthink: Adaptive thinking preferences for reasoning language model. *arXiv preprint arXiv:2506.18237*, 2025. 4

[36] Ke Wang, Junting Pan, Weikang Shi, Zimu Lu, Houxing Ren, Aojun Zhou, Mingjie Zhan, and Hongsheng Li. Measuring multimodal mathematical reasoning with math-vision dataset. In *The Thirty-eight Conference on Neural Information Processing Systems Datasets and Benchmarks Track*, 2024. 6

[37] Wenbin Wang, Liang Ding, Minyan Zeng, Xiabin Zhou, Li Shen, Yong Luo, and Dacheng Tao. Divide, conquer and combine: A training-free framework for high-resolution image perception in multimodal large language models. *arXiv preprint*, 2024. 6

[38] Ye Wang, Qianglong Chen, Zejun Li, Siyuan Wang, Shijie Guo, Zhirui Zhang, and Zhongyu Wei. Simple o3: Towards interleaved vision-language reasoning. *arXiv preprint arXiv:2508.12109*, 2025. 4, 10

[39] Jason Wei, Maarten Bosma, Vincent Y Zhao, Kelvin Guu, Adams Wei Yu, Brian Lester, Nan Du, Andrew M Dai, and Quoc V Le. Finetuned language models are zero-shot learners. *arXiv preprint arXiv:2109.01652*, 2021. 10

[40] Jason Wei, Xuezhi Wang, Dale Schuurmans, Maarten Bosma, Fei Xia, Ed Chi, Quoc V Le, Denny Zhou, et al. Chain-of-thought prompting elicits reasoning in large language models. *Advances in neural information processing systems*, 35:24824–24837, 2022. 2, 4

[41] Chenfei Wu, Shengming Yin, Weizhen Qi, Xiaodong Wang, Zecheng Tang, and Nan Duan. Visual chatgpt: Talking, drawing and editing with visual foundation models. *arXiv preprint arXiv:2303.04671*, 2023. 4

[42] Penghao Wu and Saining Xie. V?: Guided visual search as a core mechanism in multimodal llms. In *Proceedings of the IEEE/CVF Conference on Computer Vision and Pattern Recognition*, pages 13084–13094, 2024. 4, 6

[43] Siye Wu, Jian Xie, Yikai Zhang, Aili Chen, Kai Zhang, Yu Su, and Yanghua Xiao. Arm: Adaptive reasoning model. *arXiv preprint arXiv:2505.20258*, 2025. 4

[44] Wenyi Xiao and Leilei Gan. Fast-slow thinking grpo for large vision-language model reasoning. In *The Thirty-ninth Annual Conference on Neural Information Processing Systems*, 2025. 4

[45] Zhengyuan Yang, Linjie Li, Jianfeng Wang, Kevin Lin, Ehsan Azarnasab, Faisal Ahmed, Zicheng Liu, Ce Liu, Michael Zeng, and Lijuan Wang. Mm-react: Prompting chatgpt for multimodal reasoning and action. *arXiv preprint arXiv:2303.11381*, 2023. 4

[46] Huanjin Yao, Jiaxing Huang, Wenhao Wu, Jingyi Zhang, Yibo Wang, Shunyu Liu, Yingjie Wang, Yuxin Song, Haocheng Feng, Li Shen, et al. Mulberry: Empowering mllm with o1-like reasoning and reflection via collective monte carlo tree search. *arXiv preprint arXiv:2412.18319*, 2024. 11

[47] Shunyu Yao, Jeffrey Zhao, Dian Yu, Nan Du, Izhak Shafran, Karthik Narasimhan, and Yuan Cao. React: Synergizing reasoning and acting in language models. *arXiv preprint arXiv:2210.03629*, 2022. 4

[48] Edward Yeo, Yuxuan Tong, Morry Niu, Graham Neubig, and Xiang Yue. Demystifying long chain-of-thought reasoning in llms. *arXiv preprint arXiv:2502.03373*, 2025. 4

[49] Qiying Yu, Zheng Zhang, Ruofei Zhu, Yufeng Yuan, Xiaochen Zuo, Yu Yue, Weinan Dai, Tiantian Fan, Gaohong Liu, Lingjun Liu, et al. Dapo: An open-source

llm reinforcement learning system at scale. *arXiv preprint arXiv:2503.14476*, 2025. 8

[50] Jiajie Zhang, Nianyi Lin, Lei Hou, Ling Feng, and Juanzi Li. Adaptthink: Reasoning models can learn when to think. *arXiv preprint arXiv:2505.13417*, 2025. 4

[51] Renrui Zhang, Dongzhi Jiang, Yichi Zhang, Haokun Lin, Ziyu Guo, Pengshuo Qiu, Aojun Zhou, Pan Lu, Kai-Wei Chang, Yu Qiao, et al. Mathverse: Does your multi-modal llm truly see the diagrams in visual math problems? In *European Conference on Computer Vision*, pages 169–186. Springer, 2024. 6

[52] Xiang Zhang, Juntai Cao, and Chenyu You. Counting ability of large language models and impact of tokenization. *arXiv preprint arXiv:2410.19730*, 2024. 4

[53] Xintong Zhang, Zhi Gao, Bofei Zhang, Pengxiang Li, Xiaowen Zhang, Yang Liu, Tao Yuan, Yuwei Wu, Yunde Jia, Song-Chun Zhu, et al. Chain-of-focus: Adaptive visual search and zooming for multimodal reasoning via rl. *arXiv preprint arXiv:2505.15436*, 2025. 2

[54] Xiaoyun Zhang, Jingqing Ruan, Xing Ma, Yawen Zhu, Haodong Zhao, Hao Li, Jiansong Chen, Ke Zeng, and Xunliang Cai. When to continue thinking: Adaptive thinking mode switching for efficient reasoning. *arXiv preprint arXiv:2505.15400*, 2025. 4

[55] Yi-Fan Zhang, Xingyu Lu, Shukang Yin, Chaoyou Fu, Wei Chen, Xiao Hu, Bin Wen, Kaiyu Jiang, Changyi Liu, Tianke Zhang, et al. Thyme: Think beyond images. *arXiv preprint arXiv:2508.11630*, 2025. 2, 10

[56] Yuze Zhao, Jintao Huang, Jinghan Hu, Xingjun Wang, Yunlin Mao, Daoze Zhang, Zeyinzi Jiang, Zhikai Wu, Baole Ai, Ang Wang, Wenmeng Zhou, and Yingda Chen. Swift:a scalable lightweight infrastructure for fine-tuning, 2024. 6

[57] Ziwei Zheng, Michael Yang, Jack Hong, Chenxiao Zhao, Guohai Xu, Le Yang, Chao Shen, and Xing Yu. Deepeyes: Incentivizing "thinking with images" via reinforcement learning. *arXiv preprint arXiv:2505.14362*, 2025. 2, 4, 6, 7, 10, 11

[58] Xin Zou, Yizhou Wang, Yibo Yan, Yuanhuiyi Lyu, Kening Zheng, Sirui Huang, Junkai Chen, Peijie Jiang, Jia Liu, Chang Tang, et al. Look twice before you answer: Memory-space visual retracing for hallucination mitigation in multimodal large language models. *arXiv preprint arXiv:2410.03577*, 2024. 2